Signatures of spinorial order in URu_2Si_2: Landau-Ginzburg theory of hastatic order

Milan Kornjača[1], Rebecca Flint[1*],

1 Department of Physics and Astronomy, Iowa State University, 12 Physics Hall, Ames, Iowa 50011, USA

* flint@iastate.edu

July 12, 2021

Abstract

The hidden order in URu_2Si_2 remains a compelling mystery after more than thirty years, with the order parameter still unidentified. One intriguing proposal for the phase has been hastatic order: a symmetry breaking heavy Fermi liquid with a spinorial hybridization that breaks *both* single and double time-reversal symmetry. Hastatic order is the first *spinorial*, rather than vectorial order in materials, but previous work has not yet found direct consequences of the spinorial nature. In this paper, we revisit the hastatic proposal within Landau-Ginzburg theory. Rather than a single spinorial order parameter breaking double-time-reversal symmetry, we find two gauge invariant vectorial orders: the expected composite order with on-site moments, and a new quantity capturing symmetries broken solely by the spinorial nature. We address the effect of fluctuations and disorder on the tetragonal symmetry breaking, explaining the absence of in-plane moments in URu_2Si_2 and predicting a new transition in transverse field.

Contents

1 Introduction

URu_2Si_2 is an Ising heavy fermion material that undergoes a phase transition into an unknown state, known as "hidden order" (HO) at $T_{HO} = 17.5K$ [1–8]. While the large entropy at the transition suggests a large order parameter [1], no large moments have ever been found. Translation symmetry is clearly broken [9–11], but other broken symmetries [12, 13], particularly tetragonal symmetry are more controversial [14–19], with apparently conflicting results. The problem has given rise to a number of fascinating theoretical proposals [13,20–32], in part driven by the difficulty in determining the appropriate underlying microscopic model in actinide materials.
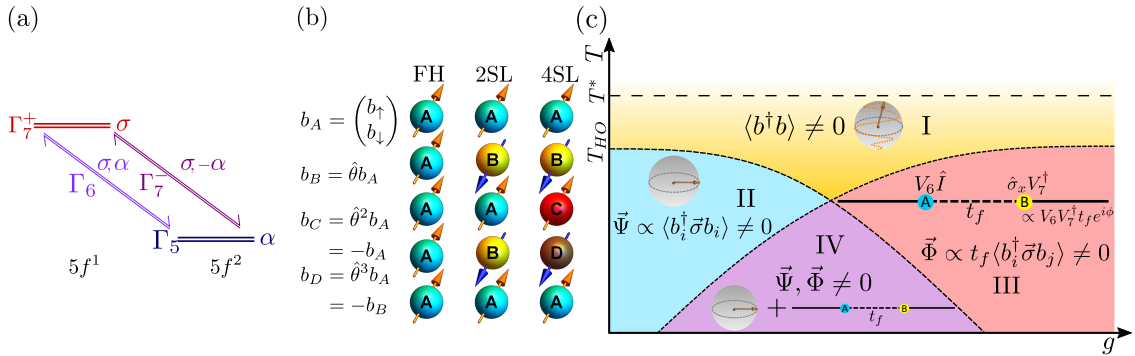

Figure 1: (a) Hastatic order arises from valence fluctuations between the U^{4+} ground state Γ_5 non-Kramers doublet and an excited Γ_7^+ Kramers doublet that lead to two-channel Kondo physics, in which the finite excited state occupation (b_σ) breaks $SU(2)$ channel symmetry. (b) As the order parameter is fundamentally a spinor, distinct spinor arrangements (color) break different symmetries, even with identical moment structure (arrows). This can be seen in the two and four sublattice antiferrohastatic phases, which break time-reversal and inversion symmetries, respectively. (c) Generic phase diagram of antiferrohastatic order beyond mean-field theory. The spinor amplitude can onset gradually with a coherence temperature T^*, followed by second order transitions for the two possible order parameters, $\vec{\Psi}$ representing the moment ordering and $\vec{\Phi}$ representing RKKY hopping induced inter-sublattice correlations, with three ordered phases: $\vec{\Psi}$ only (II), $\vec{\Phi}$ only (III) and mixed (IV).

Hastatic order was proposed to explain the HO as a symmetry breaking heavy Fermi liquid, where the order parameter is the hybridization gap itself, and the moments are nat-

urally suppressed by T_{HO}/D, where D is the conduction electron bandwidth [31,33]. This hybridization is generated by valence fluctuations from a Γ_5 non-Kramers doublet ground state to an excited Kramers doublet. The order parameter may be treated as the condensation of a *spinor* of auxiliary bosons, $\langle b_{j\sigma}\rangle$ representing the excited state occupation. The amplitude, $\langle b^\dagger b\rangle$ gives an Ising anisotropic heavy Fermi liquid, capturing hybridization gaps [5–8,34] and heavy masses [1], as well as the Ising anisotropic Fermi surface magnetization [3,11,35,36] and non-linear susceptibility [4]. The direction, $\langle b^\dagger\vec{\sigma}b\rangle$ breaks symmetries, and the staggered basal plane order of these excited moments is consistent with the physics of HO. Several key open questions remain: experimentally, hastatic order predicts tiny transverse moments, $\langle b^\dagger\vec{\sigma}_\perp b\rangle$ that have not been found in neutrons [37–39], as well as an associated broken tetragonal symmetry that remains experimentally controversial [14–19,40]; theoretically, hastatic order would be the first *spinorial* order in materials, yet thus far all predicted signatures arise from the *vectorial* composite order parameter, $\langle b^\dagger\vec{\sigma}b\rangle$.

We resolve these questions by developing the Landau-Ginzburg theory for tetragonal hastatic order with Landau parameters motivated by microscopic theory [31,41]. In addition to the *on-site* moments, $\langle b_i^\dagger\vec{\sigma}b_i\rangle$, the spinorial order generically requires a second order parameter associated with *intersite* interference, $\sim\langle b_i^\dagger\vec{\sigma}b_j\rangle$ that captures the double time-reversal symmetry breaking. We revisit the tetragonal symmetry breaking to find three relevant couplings with vastly different microscopic magnitudes that reconcile the experimental literature, and show that weak in-plane anisotropy leads to soft transverse fluctuations that couple linearly to random strains. These lead to an Imry-Ma-like loss of tetragonal symmetry breaking beyond a small critical disorder that explains why neutrons find no basal plane moments, even as μSR and NMR see disordered local fields [42,43]. The fluctuations can be stiffened by external strain or transverse magnetic fields, predicting an additional ordering transition where the transverse moments develop that should be observable in neutrons or elastoresistivity under applied strain or large transverse fields.

This paper is organized as follows: we review the microscopic model and introduce the hastatic spinor in Sec. 2, and construct three gauge-independent quantities that capture the symmetries broken by hastatic order in Sec. 3. Broken symmetries and moments are further explored in Sec. 4 and used to derive an effective antiferrohastatic Landau theory in Sec. 5, where we focus on distinct signatures of tetragonal symmetry breaking and novel transverse field transitions. In Sec. 6, we examine the effect of fluctuations and disorder on tetragonal symmetry breaking before concluding in Sec. 7.

2 Microscopic model

The simplest microscopic model for tetragonal hastatic order is the infinite-U two-channel Anderson model depicted in Fig. 1(a), where local Γ_5 non-Kramers moments fluctuate to an excited Kramers doublet (Γ_7^+) via two channels of conduction electrons that lie in different tetragonal irreducible representations, Γ_6 and Γ_7^-. As we focus on the phenomenology, we take a schematic version of this Hamiltonian that captures the essential details,

$$H = \sum_{\mathbf{k}}\epsilon_{\mathbf{k}}c_{\mathbf{k}\sigma\alpha}^\dagger c_{\mathbf{k}\sigma\alpha} + \Delta E\sum_j b_{j\sigma}^\dagger b_{j\sigma} + \sum_{ij}t_{f,ij}f_{i\alpha}^\dagger f_{j\alpha} + \sum_j c_{j\sigma\alpha}^\dagger b_{j\sigma}^\dagger\left(V_6 f_{j\alpha} + V_7 f_{j-\alpha}\right) + H.c.$$

(1)

The first term describes two bands of non-interacting conduction electrons ($c_{\mathbf{k}\sigma\alpha}$) that can mix with the Γ_5 non-Kramers doublet ground state of $5f^2$ U^{4+} ($f_{j\alpha}$) via valence fluctuations to an excited Kramers doublet ($5f^1$ or $5f^3$) at energy ΔE ($b_{j\sigma}$). The original infinite-U

model is written in terms of Hubbard operators, which we have already eliminated by introducing this representation of the excited Kramers doublet by a auxiliary boson $b_{j\sigma}$, and the non-Kramers ground state by a auxiliary fermion, $f_{j\sigma}$ as derived in Ref. [[31]]. The development of hastatic order is represented by the condensation of the auxiliary bosons, which leads to the development of hybridization gaps and heavy Fermi liquid physics, in addition to the symmetry breaking aspects discussed in this work. This mean-field is exact in the large-N limit where the $SU(2)$ pseudospin of the ground state doublet (α) is generalized to $SU(N)$. Tetragonal symmetry leads to two conduction electron channels (σ) that hybridize via two different symmetries Γ_6 and Γ_7^-. We have included an "f-electron hopping" term, t_f that moves auxiliary fermions between sites, but it is important to note that this is not the bare hopping of the original f-electrons, t_f^0. Rather it is a generic emergent term generated by fluctuations. Theoretically, it can be straightforwardly obtained by decoupling the RKKY interactions explicitly in $SU(N)$ mean-field theory [44, 45], as in $U(1)$ spin liquids. [1] Excitations are confined to the Hilbert space in Fig. 1(a) by the constraint, $\sum_\sigma b_{j\sigma}^\dagger b_{j\sigma} + \sum_\alpha f_{j\alpha}^\dagger f_{j\alpha} = 1$.

A key consequence of this auxiliary particle representation is an emergent $U(1)$ gauge symmetry:

$$b_{j\sigma} \to b_{j\sigma}\mathrm{e}^{-i\xi_j}, \; f_{j\alpha} \to f_{j\alpha}\mathrm{e}^{-i\xi_j}, \; t_{f,ij} \to t_{f,ij}\mathrm{e}^{i(\xi_i - \xi_j)}. \tag{2}$$

In the large-N limit, there are two non-gauge-invariant order parameters, $b_{j\sigma}$ and $t_{f,ij}$. For simplicity, we always chose a uniform $t_{f,ij}$ that breaks no symmetries on its own. The hastatic order parameter is naively an $SU(2)$ spinor,

$$\mathbf{b}_j = |b_j|\mathrm{e}^{i\chi_j} \begin{pmatrix} \cos\frac{\theta_j}{2}\mathrm{e}^{i\phi_j/2} \\ \sin\frac{\theta_j}{2}\mathrm{e}^{-i\phi_j/2} \end{pmatrix}. \tag{3}$$

As the spinor is not gauge invariant, its spinorial nature is washed out by gauge fluctuations for any finite N, which also affects the gauge dependent t_f. As real symmetries are additionally broken, there are real order parameters, but these must be gauge invariant combinations of the original gauge dependent quantities.

3 Order parameters

The broken symmetries are captured by gauge invariant order parameters bilinear in $\mathbf{b}_j$. These are vectorial, but carry unmistakable fingerprints of their spinorial origin. As these break different symmetries, they may develop in stages beyond mean-field theory [see Fig. 2(a)].

- $n_{b,i} = \langle \mathbf{b}_i^\dagger \mathbf{b}_i \rangle$ is the on-site excited state occupation, which breaks no symmetries and mimics the single-channel Kondo effect, reproducing the heavy Fermi liquid signatures above T_{HO} [1, 7, 34].

- $\vec{\Psi}_i = \langle \mathbf{b}_i^\dagger \vec{\sigma} \mathbf{b}_i \rangle$ are the on-site moments of the excited doublet, which correspond to the $SO(3)$ composite order parameter of the two-channel Kondo model [46–49]. The arrangement of $\vec{\Psi}_i$ may break spatial symmetries, leading to ferrohastatic (FH) or antiferrohastatic (AFH) order. In tetragonal symmetry, $\vec{\Psi}$ is reducible, with $\vec{\Psi} = \Psi_z \oplus \vec{\Psi}_\perp = m\Gamma_2^+ \oplus m\Gamma_5^+$. $m\Gamma_i^+$ labels the different irreducible representations (irreps) that preserve inversion (+), translation (Γ) and break time-reversal (m); here these are the dipolar moments, $\langle J_z \rangle$ ($m\Gamma_2^+$) and $\langle \vec{J}_\perp \rangle$ ($m\Gamma_5^+$).

---

[1]Alternately t_f may be found by treating the constrained hopping of the original f-electrons, which pick up additional auxiliary boson correlations, $t_{f,ij} \sim t_f^0 \langle b_i^\dagger b_j \rangle$.

- $\vec{\Phi}_{ij} = t_{f,ij}\langle \mathbf{b}_i^\dagger \vec{\sigma} \mathbf{b}_j \rangle$ captures additional symmetries broken by the arrangement of the spinors, which generate interference between different sites, as shown in the diagram in region III of Fig. 1(c). This interference is described by the complex $\vec{\Phi}$, whose real and imaginary parts have different symmetries. $\vec{\Psi}$ is contained in $\mathrm{Re}\vec{\Phi} \otimes \mathrm{Im}\vec{\Phi}$, allowing a third order coupling. $\vec{\Phi}$ is absent for FH order, but is generic for AFH order. t_f is required for gauge invariance, and consequentially $\vec{\Phi}$ is smaller than $\vec{\Psi}$ by t_f/D, where D is the conduction electron bandwidth. Note that the emergent t_f is proportional to T_{HO}.

Note that the original hastatic proposal [31] has only $\vec{\Psi}$, and does not actually break double-time-reversal symmetry. The original hybridization structure had four sublattices, naively breaking inversion symmetry. The additional signs were absorbed into the f-fermions via a gauge transformation, and the transformed fs were assumed to have a simple t_f hopping, which implies that the original, untransformed fs had an inversion symmetry breaking t_f hopping. Essentially, the symmetry breaking of the hybridization and the f-hopping canceled to give a singlet Φ, while $\vec{\Psi}$ remained. The resulting dispersion was doubly degenerate, reflecting the double-time-reversal symmetry. In principle, this phase is always possible, but there is no a priori reason to expect it to be favored over the spinorial phases with both $\vec{\Psi}$ and $\vec{\Phi}$. Its Landau-Ginzburg physics is fully captured by $\vec{\Psi}$.

4 Broken symmetries and moments

Now we discuss these order parameters in the context of $\mathrm{URu_2Si_2}$. The hidden order is thought to have the same wave-vector as the antiferromagnetism found under pressure, as the Fermi surfaces found in de Haas-van Alphen change very little. This order is staggered between the planes, with $\mathbf{Q} = Z = [001]$. We similarly stagger $\vec{\Psi}$, with $\vec{\Psi} = mZ_2^+ \oplus mZ_5^+$, which indicates that these moments are staggered by $\mathbf{Q}$. This $\vec{\Psi}$ order corresponds to multiple spinor arrangements differentiated by $\vec{\Phi}$, see Fig. 1(b) for two examples. Here, we consider two examples that are also uniform in the plane, but with different $\hat{c}$ axis behaviors. First we consider the naive two sublattice (2SL) case, with the spinors on the two sublattices defined as $\mathbf{b}_A$ and $\mathbf{b}_B = \theta \mathbf{b}_A$, where $\theta = i\sigma_2 K$ is the time-reversal operator, with K indicating complex conjugation. As these are spinors, $\theta^2 \mathbf{b}_A = -\mathbf{b}_A$, this order is not invariant under time-reversal followed by translation (or any symmetry operation). To preserve a time-reversal-like symmetry, *four* sublattices (4SL) are required, with $\mathbf{b}_C = \theta^2 \mathbf{b}_A = -\mathbf{b}_A$ and $\mathbf{b}_D = \theta^3 \mathbf{b}_A = -\mathbf{b}_B$. Both 2SL and 4SL orders are plausible, with one breaking time-reversal uniformly and the other breaking inversion. Analogues of both appear in cubic hastatic order [50]. $\vec{\Psi}$ and $\vec{\Phi}$ are then,

$$\vec{\Psi} = \langle \mathbf{b}_A^\dagger \vec{\sigma} \mathbf{b}_A \rangle - \langle \mathbf{b}_B^\dagger \vec{\sigma} \mathbf{b}_B \rangle, \quad \vec{\Phi} = t_f \langle \mathbf{b}_A^\dagger \vec{\sigma} \mathbf{b}_B \rangle, \tag{4}$$

with corresponding momentum space versions presented in Appendix A.

We identify $\vec{\Phi}_{2SL} = (m\Gamma_2^+ \oplus m\Gamma_5^+) \oplus Z_5^+$, and $\vec{\Phi}_{4SL} = (mZ_2^- \oplus mZ_5^-) \oplus \Gamma_5^-$, where the first (second) terms are the real (imaginary) components. Again, Γ and Z indicate uniform or c-axis staggered moments, m indicates moments that break time-reversal, and $\pm$ indicates moments even or odd under inversion symmetry.

Table 1 gives the four possible order parameters and associated moments in region IV (where both $\vec{\Psi}$ and $\vec{\Phi}$ are nonzero); regions II and III have subsets of these, as $\vec{\Phi}$ or $\vec{\Psi}$ are zero, respectively.

As all region IV phases have an in-plane dipolar component, tetragonal symmetry breaking is ubiquitous when both $\vec{\Psi}$ and $\vec{\Phi}$ are nonzero, even for $\vec{\Psi}$ along $\hat{c}$. These moments

	$\Psi_z = mZ_2^+$	$\vec{\Psi}_\perp = mZ_5^+$
	staggered m_z	staggered $\vec{m}_\perp$
2SL [$\mathrm{Im}\vec{\Phi} = Z_5^+$]	$\mathrm{Re}\vec{\Phi} = m\Gamma_2^+$	$\mathrm{Re}\vec{\Phi} = m\Gamma_5^+$
staggered (Q_{xz}, Q_{yz})	uniform $\vec{m}_\perp$	uniform m_z
4SL [$\mathrm{Im}\vec{\Phi} = \Gamma_5^-$]	$\mathrm{Re}\vec{\Phi} = mZ_5^-$	$\mathrm{Re}\vec{\Phi} = mZ_2^-$
uniform $\vec{p}_\perp$	staggered $\vec{\Omega}_\perp$	staggered Ω_z

Table 1: Possible AFH phases and associated moments in region IV of Fig. 1. In region II, only $\vec{\Psi}$ moments are present, while in region III only $\mathrm{Re}\vec{\Phi}$ or $\mathrm{Im}\vec{\Phi}$ moments are nonzero. m, p, Ω refer to magnetic, electric and toroidal dipoles, respectively, while Q indicates electric quadrupoles. In-plane moments are susceptible to being washed out by disorder. The full set of primary and secondary order parameters is given in Appendix C.

are all susceptible to being washed out by disorder, and so we highlight the robust consequences of $\vec{\Phi}$ in the $\vec{\Psi}_\perp$ phase, where uniform magnetic dipoles, m_z or staggered toroidal dipoles, Ω_z are expected in 2SL and 4SL, respectively. Microscopic theory suggests that these moments are tiny, $\sim T_{HO} t_f / D^2$. Fortunately, Kerr effect or second harmonic generation measurements should be sufficiently sensitive, and Kerr measurements tantalizingly suggest that m_z develops slightly above T_{HO} [12].

5 Antiferrohastatic Landau theory

Having understood the symmetries, we now turn to the Landau theory to discuss the thermodynamic and other responses. As t_f / D suppresses the effects of $\vec{\Phi}$, we focus on the $\vec{\Psi}$ transition from region I to II. The additional transition to region IV is also second order, but is practically undetectable, as the specific heat jump is suppressed by $\sim (t_f / D)^2$ compared to the first jump, and is expected to be within the experimental noise, $\lesssim 3\,\mathrm{mJ\,mol^{-1}K^{-1}}$ (see Appendix D). We therefore consider,

$$F_\Psi = \alpha_\perp (T - T_c^\perp)|\vec{\Psi}_\perp|^2 + \alpha_z (T - T_c^z)\Psi_z^2 + u_\perp |\vec{\Psi}_\perp|^4 + u_z \Psi_z^4 - v_1 (\Psi_{\Gamma_4}^2)^2 + v_2 \Psi_z^2 |\vec{\Psi}_\perp|^2. \quad (5)$$

F_Ψ describes two independent order parameters, Ψ_z and $\vec{\Psi}_\perp$ that couple quadratically, and $\Psi_{\Gamma_4}^2 = 2\Psi_x \Psi_y$.

The parameter choices are guided by the microscopic calculations [33, 41], as discussed in Appendix E. We know that $T_c^\perp = T_c^z \equiv T_{HO}$ and that the order parameters repel ($v_2 \gg 1$). A first order transition between Ψ_z and $\vec{\Psi}_\perp$ can be induced by varying $u_z - u_\perp = u(p - p_c^0)$; pressure tunes V_6 / V_7, which induces just such a transition microscopically. The sign of v_1 determines the pinning of ϕ and nature of the tetragonal symmetry breaking.

As tetragonal symmetry is generically broken, we consider secondary ferroquadrupolar order parameters, R_{Γ_3}, R_{Γ_4} and $\vec{R}_{\Gamma_5}$ that couple linearly to strain as shown in Appendix E:

$$\epsilon_{x^2 - y^2} = \frac{g_3 R_{\Gamma_3}}{c_{11} - c_{12}}, \; \epsilon_{xy} = \frac{g_4 R_{\Gamma_4}}{2 c_{66}}, \; (\epsilon_{xz}, \epsilon_{yz}) = \frac{g_5 \vec{R}_{\Gamma_5}}{2 c_{44}}. \quad (6)$$

R_{Γ_3} and R_{Γ_4} occur naturally in the Γ_5 doublet, and couple to bilinears of $\vec{\Psi}_\perp$: $\Psi_{\Gamma_3}^2 = \Psi_x^2 - \Psi_y^2$ and $\Psi_{\Gamma_4}^2 = 2\Psi_x \Psi_y$, while $\vec{R}_{\Gamma_5}$ shear strain couples to $\Psi_z \vec{\Psi}_\perp$. These give,

$$F_R = \sum_{i=3,4,5} \left(\alpha_R^{(i)} R_{\Gamma_i}^2 + u_R^{(i)} R_{\Gamma_i}^4 \right), \quad F_{\Psi - R} = \gamma_3 R_{\Gamma_3} \Psi_{\Gamma_3}^2 + \gamma_4 R_{\Gamma_4} \Psi_{\Gamma_4}^2 + \gamma_5 \Psi_z \vec{\Psi}_\perp \times \vec{R}_{\Gamma_5}. \quad (7)$$

Finally, we consider the coupling to magnetic field, $\vec{h}$, which has $m\Gamma_2^+ \oplus m\Gamma_5^+$ symmetry, like FH order. Bilinears of $\vec{h}_\perp$ also break tetragonal symmetry: $h_{\Gamma_3}^2 = h_x^2 - h_y^2$ and $h_{\Gamma_4}^2 = 2h_x h_y$. The additional free energy terms are,

$$F_{\Psi\text{-}h} = u_h^{(1)} h_z^2 \Psi_z^2 + u_h^{(2)} |\vec{h}_\perp|^2 \Psi_z^2 + u_h^{(3)} h_z^2 |\vec{\Psi}_\perp|^2 + u_h^{(4)} |\vec{h}_\perp|^2 |\vec{\Psi}_\perp|^2 + v_h^{(3)} h_{\Gamma_3}^2 \Psi_{\Gamma_3}^2 + v_h^{(4)} h_{\Gamma_4}^2 \Psi_{\Gamma_4}^2. \quad (8)$$

The ferroquadrupolar orders also couple to $\vec{h}$ via F_{R-h}, as given in the Appendix E.

The physics of AFH order can be explored by fixing a set of parameters and minimizing the free energy to obtain temperature, pressure and transverse/longitudinal field phase diagrams, as well as thermodynamic responses across the various transitions (details in Appendix E). These quantities compare favorably to the experimental literature on URu$_2$Si$_2$, where the HO may be identified with AFH$_\perp$ ($\vec{\Psi}_\perp$) order, and the antiferromagnet (AFM) identified with AFH$_z$ (Ψ_z) order. Remember, symmetry-wise, $\vec{\Psi}$ and AFM orders are identical, but the microscopic origins give vastly different parameter sets. Notably, the calculated U $5f^2$ moments in the AFH$_z$ phase are $\sim .5\mu_B$, consistent with neutron measurements [51, 52], while the AFH $\vec{\Psi}_\perp$ phase has much smaller in-plane U 5f^3 moments $\lesssim .01\mu_B$ for a fairly substantial mixed valency ($\sim 20\%$) [31, 41].

5.1 Tetragonal symmetry breaking in URu$_2$Si$_2$.

There are two distinct in-plane AFH orders, AFH$_{x^2-y^2}$ and AFH$_{xy}$, with $\Psi_{\Gamma_3}^2$ $\Psi_{\Gamma_4}^2$ nonzero, respectively. This tetragonal symmetry breaking actually has three experimental manifestations with different Landau coefficients: the coupling to the lattice via ferroquadrupolar order parameters ($\gamma_{3,4}$); the coupling to magnetic field ($v_h^{(3,4)}$) that yields anisotropic magnetic susceptibilities; and the coupling to an electronic nematic order parameter affecting the resistivity ($\zeta_{3,4}$, not shown; see Appendix G). The connection to microscopics is particularly useful here, as the induced electric quadrupolar moments, $R_{3,4} = \gamma_{3,4}\Psi_{\Gamma_{3,4}}^2$ are tiny, even when $\Psi_{\Gamma_{3,4}}^2$ is relatively large, suggesting that the coupling constants are of order $(T_{HO}/D)^2 \sim .001$. The anisotropic field couplings, $v_h^{(3,4)}$ are similarly suppressed [33], although typically found to be an order of magnitude larger microscopically [41]. At the same time, the tetragonal symmetry breaking near the Fermi surface is of order one, which would give substantial resistivity anisotropy signatures. As we discuss below, the tetragonal symmetry breaking may be washed out by disorder, but the signals at and above the transition remain, and tetragonal symmetry breaking may be restored by applied field or strain.

The coupling to the lattice ($\gamma_{3,4}$) manifests both as tiny jumps in the relevant elastic coefficients that have not been seen [18] (see Appendix F for details), and tiny directional jumps in the thermal expansion or magnetostriction (see Appendix E); higher order terms like $R_{\Gamma_i}^2 |\Psi|^2$, neglected here are not necessarily small and give kinks in all elastic coefficients [18]. Below the transition, the small ferroquadrupolar moments lead to a orthorhombic distortion. The experimental evidence here is mixed. One x-ray experiment [15] has observed a Γ_4 ($=B_{2g} = Fmmm$ space group) distortion, but other results do not find a distortion in the HO region, but instead find the opposite ($\Gamma_3 = B_{1g} = Immm$) distortion at higher pressures, with $T_R \gg T_{HO}$ [17, 40] developing rapidly near the critical pressure between the HO and AFM. As an aside, we can straightforwardly consider this additional orthorhombicity, shown in Fig. 2(a) by giving R_{Γ_3} a transition temperature $T_{R3}(p)$ that vanishes at $p = p_R$. This independent orthorhombic transition leads to additional transitions within the $\vec{\Psi}_\perp$ phase where ϕ changes; specific heat and structural signatures are weak due to the near constant $|\vec{\Psi}_\perp|$ and small $\gamma_{3,4}$, respectively, but the transition would be visible in elastoresistivity. The close coincidence of orthorhombic and AFM transitions in pressure would be accidental in this scenario.

Unlike the small coupling to the lattice, the large coupling to electronic nematicity gives significant jumps in the elastoresistivity at T_{HO}, in $m_{11} - m_{12}$ ($\Psi_{\Gamma_3}^2$), or m_{66} ($\Psi_{\Gamma_4}^2$) [16,19] (see Appendix G); and Γ_4 nematicity captures the cyclotron mass anisotropy with heavier masses along [110] [53].
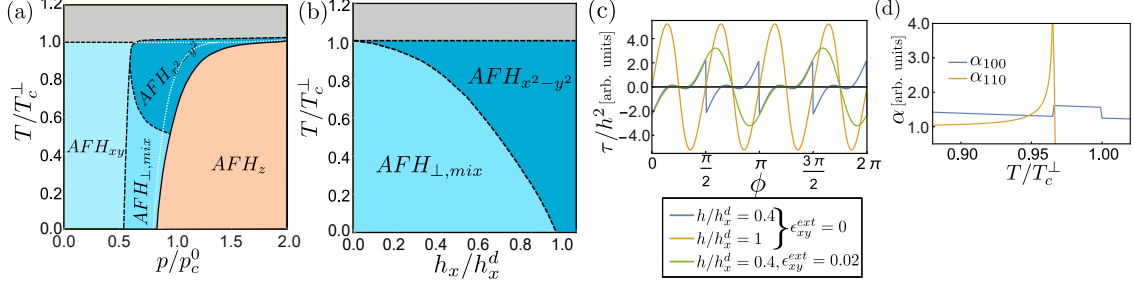

Figure 2: Transitions in the in-plane moment direction due to field or independent orthorhombic order parameters. (a) $T - p$ phase diagram including the onset of independent orthorhombicity (R_{Γ_3}) at $p \approx 0.5$; white dashed lines correspond to the original transitions. (b) $T - h_x$ phase diagram at $p = 0$, showing the field-locking transition. (c) Magnetic torque curves for different in-plane fields at $T/T_c^\perp = 0.4$, with and without small external ϵ_{Γ_4} strain. (d) Thermal expansion coefficients are sensitive to both transitions, at main hastatic transition (T_{HO}) and the field-locking transition for $h_x/h_x^d = 0.1$ ($T_c' \approx 0.96 T_{HO}$). Parameters for all plots are given in Appendix E.

The coupling to magnetic field allows the magnetic susceptibility to break tetragonal symmetry, with either $\chi_{xx} - \chi_{yy}$ or χ_{xy} nonzero for $\Psi_{\Gamma_{3,4}}^2$, respectively, as found in torque magnetometry measurements [14]. The magnetic susceptibility [14] and elastoresistivity [16] data suggest that Γ_4 symmetry breaking is favored by $v_1 > 0$.

5.2 Finite field behavior: field locking transition and torque magnetometry

To properly understand the torque magnetometry, we consider finite transverse magnetic fields in the absence of disorder. As the pinning is weak, it is possible to reorient $\vec{\Psi}_\perp$ via the quadratic coupling $v_h^{(3,4)}$. If the zero-field order is Γ_4 (AFH$_{xy}$), $\vec{h} = h_x \hat{x}$ favors the "field-locked" Γ_3 (AFH$_{x^2-y^2}$) at temperatures and fields beyond $T_c'(h_x)$. Above T_c', only $\Psi_{\Gamma_3}^2$ is present and $\Psi_{\Gamma_4}^2$ turns on via a second order transition, as shown in Fig. 2 (b).

To estimate the field-locking transition temperature and model response functions to lowest order in h_x, we use the simplified free energy,

$$F_m = \alpha_\perp(T - T_c^\perp)|\vec{\Psi}_\perp|^2 + u_\perp|\vec{\Psi}_\perp|^4 - v_1(\Psi_{\Gamma_4}^2)^2 - v_h^{(3)} h_{\Gamma_3}^2 \Psi_{\Gamma_3}^2. \tag{9}$$

We can minimize the free energy in both the high temperature field-locked phase, where the order parameter is:

$$\Psi_x^{(0)}|_{x^2-y^2} = \sqrt{-\frac{\alpha_\perp(T - T_c^\perp) - v_h^{(3)} h_x^2}{2 u_\perp}}, \; \Psi_y^{(0)}|_{x^2-y^2} = 0. \tag{10}$$

In the lower temperature mixed phase, we acquire an additional component,

$$\Psi_x^{(0)}|_{\perp,mix} = \sqrt{-\frac{\alpha_\perp(T - T_c^\perp) - v_h^{(3)}h_x^2\left(\frac{u_\perp}{v_1} - 1\right)}{4u_\perp - v_1}},$$

$$\Psi_y^{(0)}|_{\perp,mix} = \sqrt{-\frac{\alpha_\perp(T - T_c^\perp) + v_h^{(3)}h_x^2\left(\frac{u_\perp}{v_1} - 1\right)}{4u_\perp - v_1}}. \tag{11}$$

The second order transition occurs when $\Psi_y^{(0)}$ becomes nonzero, at

$$\frac{T_c'}{T_c^\perp} = 1 - \frac{v_h^{(3)}h_x^2}{\alpha_\perp T_c^\perp}\left(1 + \frac{4u_\perp}{|v_1|}\right) \approx 1 - \left(\frac{h_x}{h_z^c}\right)^2. \tag{12}$$

We estimate the $\mathcal{O}(1)$ prefactor of the field dependent term from the microscopics, as $4u_\perp/|v_1| \sim (D/T_{HO})^2$, while $v_h^{(3)}/(\alpha_\perp T_c^\perp) \sim v_h^{(3)}/[u_h^{(3)}(h_z^c)^2] \sim (T_{HO}/D)^2$. This critical field is thus proportional to the c-axis critical field, $h_z^c \approx 35$T [54], and $h_x \geq 10$T is likely required to distinguish the two transitions.

In fact, the overall magnitude of $|\Psi|$ across the phase transition is almost perfectly smooth, despite large changes in $\Psi_{x,y}$. Standard bulk probes, like specific heat, are therefore unlikely to detect this transition. Indeed, the specific heat jumps at two transitions are given by,

$$\Delta C|_{T_{HO}} = \left(-T\frac{\partial^2 F_m|_{x^2-y^2}}{\partial T^2}\right)_{T_c}, \quad \Delta C|_{T_c'} = \left(-T\frac{\partial^2\left(F_m|_{\perp,mix} - F_m|_{x^2-y^2}\right)}{\partial T^2}\right)_{T_c'}, \tag{13}$$

which indicates that the ratio of the two,

$$\frac{\Delta C|_{T_c'}}{\Delta C|_{T_c}} = \frac{v_1}{4u_\perp - v_1} \approx \frac{v_1}{4u_\perp} \approx \left(\frac{T_{HO}}{D}\right)^2, \tag{14}$$

is very small, and $\Delta C|_{T_c'}/T_c' \lesssim 0.2\,\text{mJ}\,\text{mol}^{-1}\,\text{K}^{-2}$ will be within experimental noise [55, 56] and thus undetectable.

While standard bulk probes will be blind to this transition, properties sensitive to either $\Psi_{\Gamma_3}^2$ or $\Psi_{\Gamma_4}^2$, like elastoresistivity will have larger jumps at both transitions. There will be a jump in $m_{11} - m_{12}$ at T_{HO} and in both $m_{11} - m_{12}$ and m_{66} at T_c'. These behave similarly to the thermal expansion, although the thermal expansion itself is likely difficult to detect due to the smallness of ferroquadrupolar couplings ($\gamma_{3,4} \sim (T_{HO}/D)^2$) and the possibility of multi-domain cancellation below T_{HO}.

To treat these directionally dependent quantities analytically, we include the ferroquadrupolar terms,

$$\delta F_m = \alpha_R^{(3)}R_{\Gamma_3}^2 + \alpha_R^{(4)}R_{\Gamma_4}^2 + \gamma_3 R_{\Gamma_3}\Psi_{\Gamma_3}^2 + \gamma_4 R_{\Gamma_4}\Psi_{\Gamma_4}^2, \tag{15}$$

and calculate the thermal expansion coefficients according to Appendix E to leading order in γ_3 and γ_4. Using Eq. (10)-(12), we find jumps of the same magnitude (but opposite sign) in α_{100} at both the main transition and at the field-locking one:

$$\Delta\alpha_{100}|_{T_{HO},T_c'} \approx \frac{\gamma_3}{\alpha_R^{(3)}}\left(\frac{\partial\Psi_{\Gamma_3}^2}{\partial T}\right)_{T_{HO},T_c'} \approx \pm\frac{\gamma_3}{\alpha_R^{(3)}}\frac{\alpha_\perp}{2u}, \tag{16}$$

while α_{110} shows a $(T_c' - T)^{-1/2}$ divergence only below the field-locking transition,

$$\Delta\alpha_{110}|_{T_{HO}} = 0, \qquad \alpha_{110}|_{T \to T_c'+} = 0,$$

$$\alpha_{110}|_{T \to T_c'-} \approx \frac{\gamma_4}{\alpha_R^{(4)}} \left(\frac{\partial \Psi_{\Gamma_4}^2}{\partial T}\right)_{T \to T_c'-} \approx \frac{\gamma_4}{\alpha_R^{(4)}} \frac{\alpha_\perp}{2\sqrt{2}u} \sqrt{\frac{T_c^\perp - T_c'}{T_c' - T}}. \qquad (17)$$

These are calculated numerically for the full Landau free energy and shown in Fig. 2(d).

The pinning also affects the torque magnetometry at lower fields, which is used to measure the magnetic susceptibility matrix elements. We numerically simulate torque curves with our full $\vec{\Psi}$ free energy using:

$$\vec{\tau} = \vec{M} \times \vec{h} = -\frac{\partial F}{\partial \vec{h}} \times \vec{h}, \qquad (18)$$

with results shown in Fig. 2(c). For a system with pure $\mathbb{Z}_4$ pinning, hysteretic behavior is found for $h_x < h_x^d(T)$. For larger fields, above the field-locking critical field there is no longer a two-fold component of the torque and the torque curves are entirely four-fold in character as the order parameter "follows" the field. Experiments, however, have shown a substantial, but smooth two-fold anisotropic response, although only in small crystals, where it has been attributed to the $\mathbb{Z}_2$ pinning effects of surface strains. We include these strains as an external Γ_4 strain (ϵ_{xy}^{ext}) that couples as $\delta F_\epsilon^{ext} = -\lambda_{xy}\epsilon_{xy}^{ext}\Psi_{\Gamma_4}^2$ and replaces the hysteresis by a two-fold anisotropic response similar to the experiment.

6 Fluctuations and disorder

While the weak pinning already affects the mean-field physics, it is even more important when discussing fluctuations. The in-plane moments are governed by a 3D XY model with weak $\mathbb{Z}_4$ pinning [57], where we estimate the pinning for URu$_2$Si$_2$, $v_1/u_\perp \sim (T_{HO}/D)^2 \sim .001$ for $T_{HO}/D \sim 1/30$ [31, 41]. The 3D XY model is well known to be disordered by infinitesimal random fields that couple linearly to the massless transverse fluctuations [58, 59], and here we will show that the AFH $\vec{\Psi}_\perp$ does couple linearly to random strains: the fluctuations of Γ_4 order (AFH$_{xy}$) couple to uniform Γ_3 strains, and vice versa for Γ_3 (AFH$_{x^2-y^2}$) order. Thus, we expect the in-plane order to be lost if disorder is stronger than the pinning [60–62]. It is important to note that hastatic order itself survives, even in the XY limit, as the moments are not pre-formed, like in the pure XY spin model. Instead, the hastatic moment magnitude develops ($\langle b^\dagger b\rangle$) and choose to lie in the XY plane ($|\vec{\Psi}_\perp|$) at T_c, with large barriers for out of plane fluctuations. Even the barriers for translation symmetry breaking are large, and so the AFH nature is also robust. Therefore, most signatures of hastatic order will remain, with only the tetragonal symmetry breaking washed out by disorder.

We can examine this process within Landau-Ginzburg theory, where we will focus on only the $\vec{\Psi}$ terms,

$$\mathcal{L} = c_\perp \left|\nabla\vec{\Psi}_\perp\right|^2 + c_z (\nabla\Psi_z)^2 + r_\perp|\vec{\Psi}_\perp|^2 + r_z\Psi_z^2 - \sum_{i=3,4} \left(\lambda_i\epsilon_{\Gamma_i} + v_h^{(i)}h_{\Gamma_i}^2\right) \vec{\Psi}_{\Gamma_i}^2$$

$$+ u_\perp|\vec{\Psi}_\perp|^4 + u_z\Psi_z^4 - v_1(\Psi_{\Gamma_4}^2)^2 + v_2\Psi_z^2|\vec{\Psi}_\perp|^2, \qquad (19)$$

where $r_\perp = \alpha_\perp(T - T_c^\perp)$ and $r_z = \alpha_z(T - T_c^z)$. We expand around the AFH_{xy} ground state, initially with no external strain, ϵ_{Γ_i} or field, $\vec{h}$. We write $\vec{\Psi} = (\Psi_0 + \delta\Psi_l + \delta\Psi_t, \Psi_0 +$

$\delta\Psi_l - \delta\Psi_t, \delta\Psi_z)$, with $\Psi_0 = \sqrt{-\frac{r_\perp}{4u_\perp - v_1}}$. Here, we have decomposed the fluctuations into longitudinal ($\delta\Psi_l$), in-plane transverse ($\delta\Psi_t$) and out of plane transverse ($\delta\Psi_z$). Note that expanding around the $AFH_{x^2-y^2}$ state gives similar results, where the role of Γ_3 and Γ_4 strains will be swapped. We now expand to second order in the fluctuation fields, using

$$
\begin{aligned}
\left|\vec{\Psi}_\perp\right|^2 &\approx 2\Psi_0^2 + 2(\delta\Psi_l)^2 + 2(\delta\Psi_t)^2 + 4\Psi_0\delta\Psi_l, \\
\left|\vec{\Psi}_\perp\right|^4 &\approx 4\Psi_0^4 + 24\Psi_0^2(\delta\Psi_l)^2 + 16\Psi_0^3\delta\Psi_l + 8\Psi_0^2(\delta\Psi_t)^2, \\
(\Psi_{\Gamma_4}^2)^2 &\approx \Psi_0^4 + 6\Psi_0^2(\delta\Psi_l)^2 - 2\Psi_0^2(\delta\Psi_t)^2 + 4\Psi_0^3\delta\Psi_l.
\end{aligned}
\tag{20}
$$

The three fluctuation fields completely decouple, $\mathcal{L} = \mathcal{L}[\delta\Psi_z] + \mathcal{L}[\delta\Psi_l] + \mathcal{L}[\delta\Psi_t]$, with

$$
\begin{aligned}
\mathcal{L}[\delta\Psi_z] &= c_z(\nabla\delta\Psi_z)^2 + \left(r_z - 2v_2\frac{r_\perp}{4u_\perp - v_1}\right)(\delta\Psi_z)^2, \\
\mathcal{L}[\delta\Psi_l] &= c_\perp(\nabla\delta\Psi_l)^2 - 2r_\perp(\delta\Psi_l)^2, \\
\mathcal{L}[\delta\Psi_t] &= c_\perp(\nabla\delta\Psi_t)^2 - \frac{r_\perp v_1}{4u_\perp - v_1}(\delta\Psi_t)^2.
\end{aligned}
\tag{21}
$$

The masses of the fluctuation fields can be read off directly, using that an action with $c(\nabla\phi)^2 + \beta\phi^2$ corresponds to scalar field of mass $m[\phi] = \sqrt{\beta/c}$. We find two "heavy" fluctuation fields with comparable masses ($\delta\Psi_z$ and $\delta\Psi_l$) and one "light" field ($\delta\Psi_t$), with mass ratios,

$$
\begin{aligned}
\frac{m_z}{m_l} &= \sqrt{\frac{\left|r_z - 2v_2\frac{r_\perp}{4u_\perp - v_1}\right|}{|2r_\perp|}\frac{c_\perp}{c_z}} \approx \sqrt{\left(\frac{2v_2}{4u_\perp - |v_1|} - \frac{1}{2}\right)\frac{c_\perp}{c_z}} \sim \mathcal{O}(1), \\
\frac{m_t}{m_l} &= \sqrt{\frac{|v_1|}{4u_\perp - |v_1|}} \approx \sqrt{\frac{|v_1|}{4u_\perp}} \sim \mathcal{O}\left(\frac{T_{HO}}{D}\right).
\end{aligned}
\tag{22}
$$

These fluctuations have large coherence lengths, $\xi_t/\xi_l = m_l/m_t \sim \mathcal{O}(D/T_{HO}) \sim 100$ unit cells. [2]. Note that a similar analysis can also be done in the AFH_z phase including $\vec{\Phi}$, where $\vec{\Phi}$ breaks tetragonal symmetry and has similarly light transverse in-plane fluctuations.

Next we consider the coupling of these light transverse fluctuations to strain,

$$
\mathcal{L}_{\Psi-\epsilon} = \lambda_3\epsilon_{\Gamma_3}\Psi_{\Gamma_3}^2 + \lambda_4\epsilon_{\Gamma_4}\Psi_{\Gamma_4}^2.
\tag{23}
$$

Expanding in terms of light fluctuations using $\Psi_{\Gamma_3}^2 \approx 4\Psi_0\delta\Psi_t$ and Eq. (20) for $\Psi_{\Gamma_4}^2$, we find that the light transverse fluctuations couple linearly to Γ_3 strain, as

$$
\mathcal{L}_{\delta\Psi_t-\epsilon_{\Gamma_3}} = 4\lambda_3\Psi_0\epsilon_{\Gamma_3}\delta\Psi_t,
\tag{24}
$$

to leading order in $\delta\Psi_t$. Thus, for [110] pinning, we find that the light transverse fluctuations couple linearly to random ϵ_{Γ_3} strain, but quadratically to random ϵ_{Γ_4} strain; the situation is reversed for [100] pinning.

Following the original argument of Imry and Ma [58], we consider how random strains can disorder the in-plane order. While the overall mean $\langle\epsilon_{\Gamma_3}\rangle = 0$, the local average over any finite region of volume L^d is nonzero and scales as $\langle\Delta\epsilon_{\Gamma_3}^2\rangle \sim \alpha^2 L^d$, where α parameterizes the disorder strength. This finite region can therefore gain an energy $aL^{d/2}$ (with $a \sim \lambda_3\Psi_0\alpha$) by forming a domain where $\delta\Psi_t$ aligns with the average local random

---

[2]We expect T_{HO}/D to take values in range 0.01-0.03 as it determines the degree of mixed valence.

field. Domain walls of length L cost an energy cL^{d-1}, where $c \sim m_t^2$, giving an overall domain cost, $\Delta E_d(L) = -aL^{3/2} + cL^2$, where we set $d = 3$. As long as disorder is sufficiently weak, for $L < L_0 \sim (a/c)^2$, the transverse fluctuations, $\delta\Psi_t$ align with the local average strain and order is lost on these shorter length scales, where L_0 acts as a new, larger coherence length. For stronger disorder, the full random field four-state clock model should be treated [61]; we simply assume that the tetragonal ordering temperature, $T_I(\alpha)$ decreases monotonically from T_{HO} for $\alpha = 0$ to zero at α_c, where $\alpha_c \sim c \sim m_t^2$. Therefore, as external Γ_4 or $h_{[110]}$ are applied, m_t increases and $T_I(\vec{h}_\perp)$ can rise from zero beyond a critical field to eventually meet T_{HO}, as shown in Fig. 3. Note that the field-locking transition previously discussed is completely washed out if the zero-field ground state is disordered, as the smaller barrier does not increase with field.

If samples are sufficiently disordered, $\alpha > \alpha_c$ the in-plane moments will be disordered, consistent with neutron measurements [37–39] and the absence of χ_{xy} and similar signals in larger samples [14]. Moreover, the remaining random local fields would be consistent with μSR [63] and NMR [42].

Most interestingly, m_t and thus α_c can be enhanced substantially by external strain (ϵ_i) or transverse field ($\vec{h}_\perp$), making it possible to increase $\alpha_c > \alpha$. This increase causes a transition where $\vec{\Psi}_\perp$ itself orders, always breaking more symmetries than were applied. We label this transition with $T_I(\epsilon_i, \vec{h}_\perp)$ This transition is likely difficult to observe with non-symmetry-breaking signals, just like the field locking transition, but should be visible in torque magnetometry, elastoresistivity and neutron diffraction, although the staggered moments remain very small.
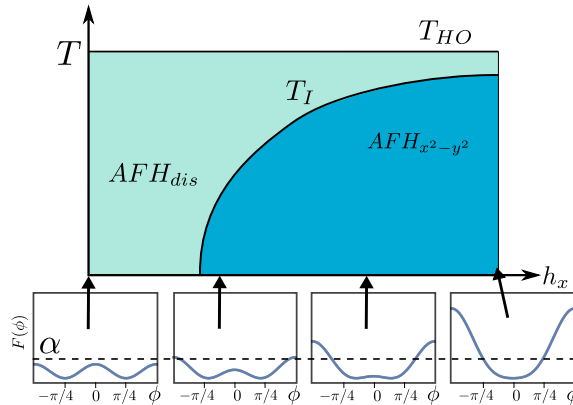

Figure 3: (Top) A cartoon phase diagram in transverse field (h_x) with random strain disorder (α) strong enough to wash out the zero-field tetragonal symmetry breaking. In-plane moments form at T_{HO}, where most hastatic signatures onset, but do not order until the magnetic field sufficiently increases the largest barrier between minima in $F(\phi)$, which occurs at $T_I(h_x)$. (Bottom) Sketches of the free energy dependence as a function of ϕ for different h_x, showing the evolution of the barrier heights.

7 Conclusion

In this paper, we showed that AFH order supports not a single, spinorial order parameter, $\langle b_{j\sigma} \rangle$ but three conventional order parameters: the scalar amplitude, n_b that develops as a crossover and induces a heavy Fermi liquid; the on-site moment, $\vec{\Psi}$ that breaks symmetries like an AFM, but with significantly different Landau parameters; and intersite interference terms, $\vec{\Phi}$ that isolate the signatures of the underlying spinorial nature. We discussed how

the weak coupling of $\vec{\Psi}$ to the lattice compared to electronic quantities reconciles disparate experimental measurements of tetragonal symmetry breaking at the transition. Finally, we argued that weak pinning leads to soft transverse fluctuations that couple linearly to random strains and may disorder the in-plane moments, without totally destroying the order. We predict that the moments can be restored by stiffening the fluctuations via transverse field, with a new transition visible in elastoresistivity and neutron diffraction.

Our Landau-Ginzburg theory is consistent with previous experiments on $\mathrm{URu_2Si_2}$, and additionally predicts:

- If $\vec{\Phi}$ orders, we expect small, but robust uniform magnetic dipoles, m_z or staggered toroidal dipoles, Ω_z in the HO, for 2SL and 4SL orders, respectively; these could be seen with Kerr effect or second harmonic generation. They may onset above or below T_{HO}, and may be sample dependent, as the barriers between 2SL and 4SL are weak [41,50].

- We predict new transitions within the HO phase for large *transverse* fields. If the disorder is strong enough to wash out the tetragonal symmetry breaking at zero field, there will generically be an ordering temperature, T_I where the applied $\mathbb{Z}_2$ pinning overcomes the Imry-Ma disordering mechanism. Alternately, if the disorder is not so strong, for applied strain, [100] perpendicular to the preferred [110] orientation, there will be a field-locking transition, T_m above which the moments align with the field and below which they take an intermediate angle. Both transitions break symmetries, and give the strongest signals in elastoresistivity, not traditional thermodynamic probes.

Hastatic order is theoretically fascinating, as the spinor order breaks not only single, but double-time-reversal. Signatures of double-time-reversal symmetry breaking were absent in previous work, but are now captured by $\vec{\Phi}$. This new order parameter can also be present in cubic hastatic order, which may be relevant for $\mathrm{PrTi_2Al_{20}}$ under pressure [50,64] or other materials. Future work may explore the interplay of double-time-reversal symmetry breaking with superconductivity and defects [49].

Acknowledgements

A Momentum space order parameters

In the main text, we derived the antiferrohastatic (AFH) order parameters in real space, but it is often convenient to derive them instead in momentum space, where the **Q** of the order can easily narrow down plausible order parameters. We begin with the real space

gauge invariant quantities, $\vec{\Psi}_i = \langle \mathbf{b}_i^\dagger \vec{\sigma} \mathbf{b}_i \rangle$ and $\vec{\Phi}_{ij} = t_{f,ij} \langle \mathbf{b}_i^\dagger \vec{\sigma} \mathbf{b}_j \rangle$ and Fourier transform:

$$\vec{\Psi}_{\mathbf{q}} = \frac{1}{N_s} \sum_{\mathbf{k}} \langle \mathbf{b}_{\mathbf{k}+\mathbf{q}}^\dagger \vec{\sigma} \mathbf{b}_{\mathbf{k}} \rangle = \frac{1}{N_s} \sum_i \langle \mathbf{b}_i^\dagger \vec{\sigma} \mathbf{b}_i \rangle e^{i\mathbf{q}\cdot\mathbf{R}_i}, \tag{25}$$

$$\vec{\Phi}_{\mathbf{q}} = \frac{1}{N_s^2} \sum_{\mathbf{k_1},\mathbf{k_2}} t_{f,\mathbf{k_1 k_2}} \langle \mathbf{b}_{\mathbf{k_1}+\mathbf{q}}^\dagger \vec{\sigma} \mathbf{b}_{\mathbf{k_2}} \rangle = \frac{1}{N_s^2} \sum_{i,j} t_{f,ij} \langle \mathbf{b}_i^\dagger \vec{\sigma} \mathbf{b}_j \rangle e^{i\mathbf{q}\cdot\mathbf{R}_i}, \tag{26}$$

where $\vec{R}_i$ denotes the real space lattice vectors, N_s the number of sites, and we used the Fourier transforms,

$$\mathbf{b_k} = \frac{1}{\sqrt{N_s}} \sum_i e^{i\mathbf{k}\cdot\mathbf{R}_i} \mathbf{b}_i,$$

$$t_{f,\mathbf{k_1 k_2}} = \frac{1}{N_s} \sum_{i,j} e^{i(\mathbf{k_1}\cdot\mathbf{R}_i - \mathbf{k_2}\cdot\mathbf{R}_j)} t_{f,ij}. \tag{27}$$

For simplicity, we assume that $t_{f,ij} = t_f \sum_{\boldsymbol{\eta}} \delta(\mathbf{R}_i + \boldsymbol{\eta} - \mathbf{R}_j)$ is uniform and only nonzero between nearest-neighbors indicated by $\boldsymbol{\eta}$. This makes $t_{f,\mathbf{k_1},\mathbf{k_2}} = t_f \sum_{\boldsymbol{\eta}} e^{-i\mathbf{k_1}\cdot\boldsymbol{\eta}} \delta(\mathbf{k_1} - \mathbf{k_2})$, and

$$\vec{\Phi}_{\mathbf{q}} = \frac{t_f}{N_s} \sum_{\mathbf{k},\boldsymbol{\eta}} \langle \mathbf{b}_{\mathbf{k}+\mathbf{q}}^\dagger \vec{\sigma} \mathbf{b}_{\mathbf{k}} \rangle e^{-i\mathbf{k}\cdot\boldsymbol{\eta}}. \tag{28}$$

Now we turn to the specific case of URu_2Si_2, where we assume that the spinor is uniform in the plane and modulated along $\hat{z}$ as shown in Fig. 1 in the main text. Knowing that $\mathbf{Q} = [001]$, we expect that only $\langle \boldsymbol{b_0} \rangle$ is nonzero for uniform, ferrohastatic (FH) order [65], while for the two sublattice (2SL) AFH order, $\langle \boldsymbol{b_0} \rangle$ and $\langle \boldsymbol{b_Q} \rangle$ are nonzero and for the four sublattice (4SL) AFH, $\langle \boldsymbol{b_{\pm Q/2}} \rangle$ are nonzero (with $\langle \boldsymbol{b_0} \rangle$ and $\langle \boldsymbol{b_Q} \rangle$ vanishing due to the preservation of time-reversal). In simplifying the expressions, we use $2\boldsymbol{Q} = \mathbf{0}$. It is convenient to rewrite these non-zero Fourier components in terms of the real space $\mathbf{b}_A$ and $\mathbf{b}_B = \hat{\theta} \mathbf{b}_A$ for the 2SL/4SL cases:

$$\mathbf{b_0} = \frac{1}{\sqrt{2}} (\mathbf{b}_A + \mathbf{b}_B), \qquad \mathbf{b_Q} = \frac{1}{\sqrt{2}} (\mathbf{b}_A - \mathbf{b}_B), \tag{29}$$

$$\mathbf{b}_{\frac{\mathbf{Q}}{2}} = \frac{1}{\sqrt{2}} (\mathbf{b}_A + i\mathbf{b}_B), \qquad \mathbf{b}_{-\frac{\mathbf{Q}}{2}} = \frac{1}{\sqrt{2}} (\mathbf{b}_A - i\mathbf{b}_B).$$

Now we can evaluate the nonzero order parameters $\vec{\Psi}_{\boldsymbol{q}}$ and $\vec{\Phi}_{\boldsymbol{q}}$. For the FH case, only $\vec{\Psi}_{\mathbf{0}} = \langle \mathbf{b}_A^\dagger \vec{\sigma} \mathbf{b}_A \rangle$ is nonzero, as expected. The nonzero contributions for 2SL order are:

$$\vec{\Psi}^{2SL} = \mathrm{Re}\langle \mathbf{b}_{\mathbf{Q}}^\dagger \vec{\sigma} \mathbf{b}_{\mathbf{0}} \rangle,$$

$$\mathrm{Re}\vec{\Phi}^{2SL} = t_f \left(\langle \mathbf{b}_{\mathbf{0}}^\dagger \vec{\sigma} \mathbf{b}_{\mathbf{0}} \rangle - \langle \mathbf{b}_{\mathbf{Q}}^\dagger \vec{\sigma} \mathbf{b}_{\mathbf{Q}} \rangle \right),$$

$$\mathrm{Im}\vec{\Phi}^{2SL} = t_f \mathrm{Im}\langle \mathbf{b}_{\mathbf{Q}}^\dagger \vec{\sigma} \mathbf{b}_{\mathbf{0}} \rangle, \tag{30}$$

which are equivalent to real space $\vec{\Psi} = \langle \mathbf{b}_A^\dagger \vec{\sigma} \mathbf{b}_A \rangle - \langle \mathbf{b}_B^\dagger \vec{\sigma} \mathbf{b}_B \rangle$, $\mathrm{Re}\vec{\Phi} = \mathrm{Re}\langle \mathbf{b}_A^\dagger \vec{\sigma} \mathbf{b}_B \rangle$ and $\mathrm{Im}\vec{\Phi} = \mathrm{Im}\langle \mathbf{b}_A^\dagger \vec{\sigma} \mathbf{b}_B \rangle$, respectively.

The 4SL order parameters are instead:

$$\vec{\Psi}^{4SL} = \mathrm{Re}\langle \mathbf{b}_{-\frac{\mathbf{Q}}{2}}^\dagger \vec{\sigma} \mathbf{b}_{\frac{\mathbf{Q}}{2}} \rangle,$$

$$\mathrm{Re}\vec{\Phi}^{4SL} = t_f \mathrm{Im}\langle \mathbf{b}_{\frac{\mathbf{Q}}{2}}^\dagger \vec{\sigma} \mathbf{b}_{\frac{\mathbf{Q}}{2}} \rangle,$$

$$\mathrm{Im}\vec{\Phi}^{4SL} = t_f \mathrm{Im}\langle \mathbf{b}_{-\frac{\mathbf{Q}}{2}}^\dagger \vec{\sigma} \mathbf{b}_{\frac{\mathbf{Q}}{2}} \rangle, \tag{31}$$

which again correspond exactly to the real space $\vec{\Psi} = \langle \mathbf{b}_A^\dagger \vec{\sigma} \mathbf{b}_A \rangle - \langle \mathbf{b}_B^\dagger \vec{\sigma} \mathbf{b}_B \rangle$, $\text{Re}\vec{\Phi} = \text{Re}\langle \mathbf{b}_A^\dagger \vec{\sigma} \mathbf{b}_B \rangle$ and $\text{Im}\vec{\Phi} = \text{Im}\langle \mathbf{b}_A^\dagger \vec{\sigma} \mathbf{b}_B \rangle$, respectively. Thus, the real space and momentum space analyses agree.

B Composite order parameters

The complications of tetragonal symmetry make it difficult to relate $\vec{\Psi}$ and $\vec{\Phi}$ to the more familiar composite order parameter discussed in the $SU(2)$ two-channel Kondo model [46], as in tetragonal symmetry the spin and channel $SU(2)$'s are entangled. Here, we turn to the simpler two-channel Kondo model, valid for cubic symmetry, and discuss the composite forms of $\vec{\Psi}$ and $\vec{\Phi}$. The two-channel Kondo-Heisenberg model is [50],

$$H = \sum_{k\sigma\alpha} \epsilon_{\mathbf{k}} c_{\mathbf{k}\sigma\alpha}^\dagger c_{\mathbf{k}\sigma\alpha} + J_K \sum_{j\sigma\alpha\beta} c_{j\sigma\alpha}^\dagger \vec{\tau}_{\alpha\beta} c_{j\sigma\beta} \cdot \vec{\tau}_{f,j} + J_H \sum_{\langle ij \rangle} \vec{\tau}_{f,i} \cdot \vec{\tau}_{f,j} \tag{32}$$

Here, $\vec{\tau}_f$ are the local pseudospin moments (in cubic symmetry these originate from the Γ_3 non-Kramers doublet and are mainly quadrupolar), with the pseudospin degrees of freedom labeled by $\alpha, \beta = \pm$. The channel degrees of freedom are labeled by $\sigma = \uparrow$,$\downarrow$ and channel moments will be labeled by $\vec{\sigma}$. The local moments may be represented by $\vec{\tau}_f = \frac{1}{2} f_\alpha^\dagger \vec{\tau}_{\alpha\beta} f_\beta$ (introducing Einstein summation notation), which leads to a quartic Hamiltonian. In the $SU(N)$ large-N limit, this Hamiltonian can be decoupled by two kinds of Hubbard-Stratonovich fields, $b_{j\sigma} \propto \langle f_{j\alpha}^\dagger c_{j\sigma\alpha} \rangle$ and $t_{f,ij} \propto \langle f_{i\alpha}^\dagger f_{j\alpha} \rangle$. Now, the composite order parameter can be roughly derived as,

$$\begin{aligned}
\Psi_j^a &= \langle : b_{j\sigma}^\dagger \sigma_{\sigma\sigma'}^a b_{j\sigma'} : \rangle \\
&\propto \langle : c_{j\sigma\alpha}^\dagger f_{j\alpha} \sigma_{\sigma\sigma'}^a f_{j\beta}^\dagger c_{j\sigma'\beta} : \rangle \\
&\propto \langle : c_{j\sigma\alpha}^\dagger \sigma_{\sigma\sigma'}^a c_{j\sigma'\beta} f_{j\beta}^\dagger f_{j\alpha} : \rangle \\
&\propto \langle : c_{j\sigma}^\dagger \sigma_{\sigma\sigma'}^a \vec{\tau} c_{j\sigma'} \cdot \vec{\tau}_{f,j} : \rangle.
\end{aligned} \tag{33}$$

Here, we are evaluating the normal ordered operator, $\langle : O : \rangle$, and in the last line we recombine $f_\beta^\dagger f_\alpha = \vec{\tau}_f \cdot \vec{\tau}_{\beta\alpha}$, use $\text{Tr}\tau^a\tau^b = 2\delta^{ab}$ and suppress the α, β indices in the on-site conduction electron spin density. Here, we have recovered the familiar composite order parameter [46], which is interpreted as a channel dependent Kondo singlet - e.g. - the conduction electron pseudospin density screens the local moment, but has a leftover $SU(2)$ channel degree of freedom. Now we can perform the same procedure for $\vec{\Phi}$.

$$\begin{aligned}
\Phi_{ij}^a &= \langle : t_{f,ij} b_{i\sigma}^\dagger \vec{\sigma}_{\sigma\sigma'} b_{j\sigma'} : \rangle \\
&\propto \langle : f_{i\alpha}^\dagger f_{j\alpha} c_{i\sigma\beta}^\dagger f_{i\beta} \sigma_{\sigma\sigma'}^a f_{j\gamma}^\dagger c_{j\sigma'\gamma} : \rangle \\
&\propto \langle : f_{i\alpha}^\dagger f_{i\beta} c_{i\sigma\beta}^\dagger \sigma_{\sigma\sigma'}^a c_{j\sigma'\gamma} f_{j\gamma}^\dagger f_{j\alpha} : \rangle \\
&\propto i\langle : \vec{\tau}_{f,i} \cdot \left(c_{i\sigma}^\dagger \sigma_{\sigma\sigma'}^a \vec{\tau} c_{j\sigma'} \times \vec{\tau}_{f,j} \right) : \rangle
\end{aligned} \tag{34}$$

We now use $\text{Tr}\tau^a\tau^b\tau^c = 2i\epsilon^{abc}$. The relevant conduction electron quantity is now a pseudospin dependent hopping term that forms a triple product with the local pseudospin moments at each site.

C   Secondary order parameters and moments

The primary order parameters ($\vec{\Psi}$ and $\vec{\Phi}$) and the associated broken symmetries and moments were discussed in the main text. Here we report the secondary order parameters coming from $\vec{\Psi} \otimes \vec{\Psi}$, $\vec{\Phi} \otimes \vec{\Psi}$ and $\vec{\Phi} \otimes \vec{\Phi}$, which could be used to construct a more general AFH free energy. Table 2 contains all of the secondary order parameters, their symmetries and associated moments, for the FH, simple AFH ($t_f = 0$), 2SL and 4SL phases. There are no new symmetries that can be constructed from three or more order parameters. Note that $\vec{\Phi}$ is expected to be smaller than $\vec{\Psi}$ by a factor of t_f/D, which also suppresses the secondary moments and makes them more difficult to detect.

$\vec{\Psi} \otimes \vec{\Psi}$ contains only non-time-reversal symmetry breaking electric quadrupole moments that capture the broken tetragonal symmetry, and have been substantially discussed in the main text.

$\vec{\Psi} \otimes \vec{\Phi}$ is substantially redundant with $\vec{\Phi}$ itself, however, in the XY AFH phases, there are additional moments. Particularly, for the 2SL XY phase, the uniform time-reversal symmetry breaking is additionally indicated by $m\Gamma_1^+$ (a dotriacontapolar order parameter) and tetragonal symmetry breaking octupolar moments, $m\Gamma_{3,4}^+$. For the 4SL XY phase, the inversion symmetry breaking is indicated by staggered magnetic quadrupoles that both break ($mZ_{3,4}^-$) and preserve (mZ_1^-) tetragonal symmetry. These higher order moments might be useful signatures of the inversion symmetry breaking, as the uniform electric dipole moments, p_z of the phase will be screened in a metal.

$\vec{\Phi} \otimes \vec{\Phi}$ contains the smallest secondary order parameters, suppressed by $(t_f/D)^2$, but are particularly interesting in the 2SL/4SL Z phases, which would correspond to the large moment antiferromagnet. Here, the $\vec{\Phi} \otimes \vec{\Phi}$ moments break tetragonal symmetry even though $\vec{\Psi}$ does not, with the same uniform quadrupole moments as contained in $\vec{\Psi} \otimes \vec{\Psi}$ for the XY phases. Note that these moments are also susceptible to the Imry-Ma disordering mechanism, and are unlikely to be detectable.

When considering moment directions, it is useful to keep in mind that in the large-N, mean-field limit, the angular dependence of the order parameters can be written explicitly as:

$$\vec{\Psi} = |b|^2 (\sin\theta\cos\phi, \sin\theta\sin\phi, \cos\theta)$$
$$\mathrm{Re}\vec{\Phi} = t_f |b|^2 (\cos\theta\cos\phi, \cos\theta\sin\phi, -\sin\theta)$$
$$\mathrm{Im}\vec{\Phi} = t_f |b|^2 (\sin\phi, -\cos\phi, 0). \tag{35}$$

These are mutually orthogonal, although this condition may be relaxed for finite N, where they may also develop at different temperatures. The triple product of these is an angle-independent scalar, and there are in fact two distinct third order invariants (Γ_1^+) that can be constructed in tetragonal symmetry: $\Psi_z(\mathrm{Re}\vec{\Phi}_\perp \times \mathrm{Im}\vec{\Phi})_z$ and $\mathrm{Re}\Phi_z(\vec{\Psi}_\perp \times \mathrm{Im}\vec{\Phi})_z$, which are relevant for either the Z or XY phases respectively. These third order terms cause the hastatic order transition to be first order at the multicritical point, but do not generically lead to first order transitions and have no other qualitative effects.

D   Specific heat jump upon transition to region IV

In the main text, we mainly consider the signatures of T_Ψ and neglect signatures at T_Φ. Here we justify this. If we assume $T_\Psi > T_\Phi$, the second specific heat jump associated with T_Φ is expected to be reduced by at least a factor of $(t_f/D)^2$, as $\Delta C_V = \alpha_{\Psi,\Phi}^2 T_{HO}/u_{\Psi,\Phi} = \alpha_{\Psi,\Phi}(\Psi,\Phi)_{T=0}^2$, and we know $\Phi_{T=0} \approx \frac{t_f}{D}\Psi_{T=0}$. We roughly estimate

Table 2: Possible hastatic phases, their symmetries and their moments. Order parameter (OP) irreducible representations (irreps) are labeled as $\Gamma(Z)_i$ corresponding to particular symmetry under spatial rotations, with Γ and Z giving the behavior under translation (Γ is uniform, Z staggered with $\mathbf{Q} = Z = [001]$). In addition, the prefix m is used to denote time-reversal breaking, while the superscript $+(-)$ is used to denote parity under inversion. Only the symmetry breaking order parameters and moments are shown (Γ_1+ are dropped). For each order parameter irrep, only the lowest order multipolar moments are indicated. Magnetic dipolar moments are labeled by $\vec{m}_\perp$ (in plane) and m_z (along z-axis), electric dipolar by $\vec{p}$, toroidal dipolar by $\vec{\Omega}$, electric quadrupolar by Q, magnetic quadrupolar by M, magnetic octupolar by T and magnetic dotriacontapolar by D. Less common octupoles and dotriacontapoles are defined in terms of angular momentum tensors as $T_{xyz} = \overline{\langle J_x J_y J_z \rangle}$, $T_z^\beta = \overline{\langle (J_x^2 - J_y^2) J_z \rangle}$ and $D_4 = \overline{\langle J_x J_y (J_x^2 - J_y^2) J_z \rangle}$, where the overline indicates symmetrization. The relative sizes of the moments are not denoted, although they are expected to decrease between rows (for details, see the main text of this Appendix).

	FH	AFH ($t_f = 0$)	2SL AFH (Z)	2SL AFH (XY)	4SL AFH (Z)	4SL AFH (XY)
Primary OPs						
$\vec{\Psi}$	$m\Gamma_2^+ \oplus m\Gamma_5^+$ uniform m_z and $\vec{m}_\perp$	$mZ_2^+ \oplus mZ_5^+$ staggered m_z and $\vec{m}_\perp$	mZ_2^+ staggered m_z	mZ_5^+ staggered $\vec{m}_\perp$	mZ_2^+ staggered m_z	mZ_5^+ staggered $\vec{m}_\perp$
$\vec{\Phi}$	-	-	$m\Gamma_5^+ \oplus Z_5^+$, uniform $\vec{m}_\perp$, staggered (Q_{xz}, Q_{yz})	$m\Gamma_2^+ \oplus Z_5^+$ uniform m_z, staggered (Q_{xz}, Q_{yz})	$mZ_5^- \oplus \Gamma_5^-$ staggered $\vec{\Omega}_\perp$, uniform $\vec{p}_\perp$	$mZ_2^- \oplus \Gamma_5^-$ staggered Ω_z, uniform $\vec{p}_\perp$
Secondary OPs						
$\vec{\Psi} \otimes \vec{\Psi}$	$\Gamma_3^+ \oplus \Gamma_4^+ \oplus \Gamma_5^+$ uniform $Q_{x^2-y^2}$, Q_{xy} and (Q_{xz}, Q_{yz})	$\Gamma_3^+ \oplus \Gamma_4^+ \oplus \Gamma_5^+$ uniform $Q_{x^2-y^2}$, Q_{xy} and (Q_{xz}, Q_{yz})	-	$\Gamma_3^+ \oplus \Gamma_4^+$ uniform $Q_{x^2-y^2}$, Q_{xy}	-	$\Gamma_3^+ \oplus \Gamma_4^+$ uniform $Q_{x^2-y^2}$, Q_{xy}
$\vec{\Phi} \otimes \vec{\Psi}$	-	-	$m\Gamma_5^+ \oplus Z_5^+$ uniform $\vec{m}_\perp$ staggered (Q_{xz}, Q_{yz})	$Z_5^+ \oplus m\Gamma_1^+ \oplus m\Gamma_2^+ \oplus m\Gamma_3^+ \oplus m\Gamma_4^+$ staggered (Q_{xz}, Q_{yz}), uniform D_4, m_z, T_{xyz}, T_z^β,	$\Gamma_5^- \oplus mZ_5^-$ uniform $\vec{p}_\perp$, staggered $\vec{\Omega}_\perp$	$\Gamma_5^- \oplus mZ_1^- \oplus mZ_2^- \oplus mZ_3^- \oplus mZ_4^-$ uniform $\vec{p}_\perp$, staggered M_{z^2}, Ω_z, $M_{x^2-y^2}$, M_{xy}
$\vec{\Phi} \otimes \vec{\Phi}$	-	-	$\Gamma_3^+ \oplus \Gamma_4^+ \oplus mZ_2^+ \oplus mZ_3^+ \oplus mZ_4^+$ uniform $Q_{x^2-y^2}$, Q_{xy}, staggered m_z, T_{xyz}, T_z^β	$\Gamma_3^+ \oplus \Gamma_4^+ \oplus mZ_5^+$ uniform $Q_{x^2-y^2}$, Q_{xy}, staggered $\vec{m}_\perp$	$\Gamma_3^+ \oplus \Gamma_4^+ \oplus mZ_2^+ \oplus mZ_3^+ \oplus mZ_4^+$ uniform $Q_{x^2-y^2}$, Q_{xy}, staggered m_z, T_{xyz}, T_z^β	$\Gamma_3^+ \oplus \Gamma_4^+ \oplus mZ_5^+$ uniform $Q_{x^2-y^2}$, Q_{xy}, staggered $\vec{m}_\perp$

$t_f/D \approx T_{HO}/D \approx 1/30$ for URu$_2$Si$_2$, which means $\Delta C_V|_{T_\Phi} \lesssim .001\Delta C_V|_{T_\Psi} \approx 3$mJ/mol K, within the experimental noise. The moments are also suppressed, but may be detected by more sensitive techniques.

E Free energy parameter choices and details of the hastatic transitions

In this section we present the details of the free energy used for numerical calculation of phase diagrams and thermodynamic response across the AFH transitions. Particular emphasis is given to the parameter choices made with microscopic results [33] in mind. We also show additional details of the hastatic order transitions, including the field-locking transition.

Here, we repeat the free energy given in the main text:

$$F = F_\Psi + F_R + F_{\Psi-R} + F_{\Psi-h} + F_{R-h}, \tag{36}$$

which governs the response of the order parameter, Ψ and internal strains/ferroquadrupolar order parameters, R. The ferroquadrupolar order parameters are proportional to the elastic strain, and we derive them in detail here. The strain components in tetragonal symmetry are $\left[\epsilon_{z^2}, \epsilon_{x^2-y^2}, \epsilon_{xy}, \vec{\epsilon} = (\epsilon_{xz}, \epsilon_{yz})\right]$ which transform as $\Gamma_{1g}(A_{1g}) \oplus \Gamma_{3g}(B_{1g}) \oplus \Gamma_{4g}(B_{2g}) \oplus \Gamma_{5g}(E_g)$ and are described by the Landau free energy,

$$F_{el} = \frac{c_{11} - c_{12}}{2}\epsilon_{x^2-y^2}^2 + c_{66}\epsilon_{xy}^2 + c_{44}|\vec{\epsilon}|^2 - g_3\epsilon_{x^2-y^2}R_{\Gamma_3} - g_4\epsilon_{xy}R_{\Gamma_4} - g_5\vec{\epsilon}\cdot\vec{R}_{\Gamma_5}, \tag{37}$$

where we omit the bulk(volume) terms. After integrating out the strains from the elastic free energy we find the corresponding ferroquadrupolar orders:

$$\epsilon_{x^2-y^2} = \frac{g_3 R_{\Gamma_3}}{c_{11}-c_{12}}, \ \epsilon_{xy} = \frac{g_4 R_{\Gamma_4}}{2c_{66}}, \ \vec{\epsilon} = \frac{g_5 \vec{R}_{\Gamma_5}}{2c_{44}}, \tag{38}$$

which interact with the order parameter, $\vec{\Psi}$ and external field, $\vec{h}$ and are described by the resulting Landau theory,

$$F_\Psi = \alpha_\perp(T - T_c^\perp)|\vec{\Psi}_\perp|^2 + \alpha_z(T - T_c^z)\Psi_z^2 + u_\perp|\vec{\Psi}_\perp|^4$$
$$+ u_z\Psi_z^4 - v_1(\Psi_{\Gamma_4}^2)^2 + v_2\Psi_z^2|\vec{\Psi}_\perp|^2, \tag{39}$$

$$F_R = \sum_{i=3,4,5}\left(\alpha_R^{(i)}R_{\Gamma_i}^2 + u_R^{(i)}R_{\Gamma_i}^4\right), \tag{40}$$

$$F_{\Psi-R} = \gamma_3 R_{\Gamma_3}\Psi_{\Gamma_3}^2 + \gamma_4 R_{\Gamma_4}\Psi_{\Gamma_4}^2 + \gamma_5\Psi_z\vec{\Psi}_\perp\times\vec{R}_{\Gamma_5}. \tag{41}$$

Note that third order terms in R are allowed by symmetry, but we drop them as well as the biquadratic couplings and anisotropic fourth order terms in Eq. (7). Although allowed by symmetry, they do not qualitatively affect the physics of interest. The couplings to external field are,

$$F_{\Psi-h} = u_h^{(1)}h_z^2\Psi_z^2 + u_h^{(2)}|\vec{h}_\perp|^2\Psi_z^2 + u_h^{(3)}h_z^2|\vec{\Psi}_\perp|^2 \tag{42}$$
$$+ u_h^{(4)}|\vec{h}_\perp|^2|\vec{\Psi}_\perp|^2 + v_h^{(3)}h_{\Gamma_3}^2\Psi_{\Gamma_3}^2 + v_h^{(4)}h_{\Gamma_4}^2\Psi_{\Gamma_4}^2,$$

$$F_{R-h} = \gamma_{hR}^{(3)}h_{\Gamma_3}^2 R_{\Gamma_3} + \gamma_{hR}^{(4)}h_{\Gamma_4}^2 R_{\Gamma_4} + \gamma_{hR}^{(5)}h_z\vec{h}_\perp\times\vec{R}_{5g}. \tag{43}$$

In order to facilitate relevant discussion for the physics of hidden order in URu_2Si_2, our parameter choices for numerical optimization of free energy were heavily influenced by microscopic theories [33].

First, we discuss the parameters for F_Ψ, as given in Eq. (39). We chose parameters to reproduce the temperature-pressure phase diagram of URu_2Si_2, which is one of many microscopic possibilities. However, once chosen, we use these parameters for the rest of our calculations. As such, we fix:

- $\alpha_\perp = \alpha_z = 1$, $u_\perp = 4$ and $u_z = u_\perp + u'(p - p_c)$, with $T_c^\perp = 1$ and $T_c^z = T_c^\perp + \delta(p - p_c')^3$, where $u' = 1.$, $\delta = .1$, $p_c^0 = 2$ and $p_c' = 1.5$. These choices reproduce the pressure dependence of the transition temperatures, with $p_c' < p_c^0$ necessary to reproduce the rightward curvature of the XY/Z transition at higher temperatures. A large value of $v_2 = 12$ ensures that the transition between XY and Z orders is first order, with no coexistence. Microscopically, the pressure dependence can be induced by tuning the ratio V_6/V_7, which tunes the relative energy of XY and Z orders.

- v_1 tunes the tetragonal symmetry breaking, where $v_1 > 0$ gives the [110] in-plane pinning consistent with experiment. The pinning can be calculated in the microscopic theory, where $\frac{v_1}{4u_\perp} \sim (T_{HO}/D)^2 \sim .001$. However, this small value makes numerical calculations difficult, and so we have chosen the unphysically large value $v_1 = 1$ for convenience.

The parameters for the ferroquadrupolar components were chosen:

- $\alpha_R^{(4)} = .5$ and $\alpha_R^{(3)} = \alpha_R^{(4)} + \delta_R(T - T_R \tan^{-1}[10(p - p_R)])$, where $\delta_R = 0$ except when we considered the independent Γ_3 orthorhombic order, with $\delta_R = .5$, $p_R = .5 < p_c^0$ and $T_R = 5$, where these parameter choices give a very sharp second order transition to the $R_{\Gamma_3} \neq 0$ order at p_Q. Additionally, we took $u_R^{(3,4)} = 16$.

- While we included $\vec{R}_{\Gamma_5}$ for completeness, it is only relevant if there is XY and Z phase coexistence, which is not found experimentally (and rarely found microscopically). As such, we drop these contributions entirely.

- The coupling between strain and $\Psi_{\Gamma_{3,4}}^2$ is given by $\gamma_{3,4}$, which is found microscopically to manifest as tiny quadrupolar moments proportional to $(T_{HO}/D)^2 \sim .001$. As with v_1, this small value would make numerical calculations difficult, and so we have chosen $\gamma_{3,4} = -.5$.

Finally, the field coupling parameters were chosen primarily based on the relatively weak coupling of perpendicular compared to c-axis fields, as the c-axis field splits the non-Kramers doublet linearly, while the perpendicular fields only split it quadratically. Previous microscopic calculations [33] found that the in-plane couplings were suppressed by $(T_{HO}/D)^2$ compared to the out of plane couplings.

- The longitudinal field (h_z) coupling to Ψ_z, $u_h^{(1)} = 3.3$ is slightly larger than the coupling to $\vec{\Psi}_\perp$, $u_h^{(3)} = 3$. This difference reproduces the experimental phase diagram in h_z, where the hidden order phase is favored over the local moment antiferromagnet [66,67]. This phase diagram was also generically obtained in microscopic calculations [41].

- The isotropic in-plane field couplings were both chosen to be an order of magnitude smaller, $u_h^{(2,4)} = .1$. The difference between them is not important for any of the interesting physics. The anisotropic couplings, $v_h^{(3,4)} = -.3$ give a $\mathbb{Z}_2$ pinning of the

hastatic spinor in transverse field, which governs the maximum magnitude of the torque magnetometry. Again, we have chosen these parameters to be an order of magnitude larger than expected from the microscopics for ease of numerical calculations, where based on the torque results [14], we expect $|v_h|/u_h^{(1)} \sim \chi_{xy}/\chi_{zz} \gtrsim .01$. Note that this is likely an overestimate, as the Landau theory is only valid near the transition and the linear component of χ_{xy} in $(T_{HO} - T)$ should be extracted.

- The coupling of field to ferroquadrupolar orders was fixed to be $\gamma_{hR}^{(3,4)} = -.5$ and has little qualitative effect.
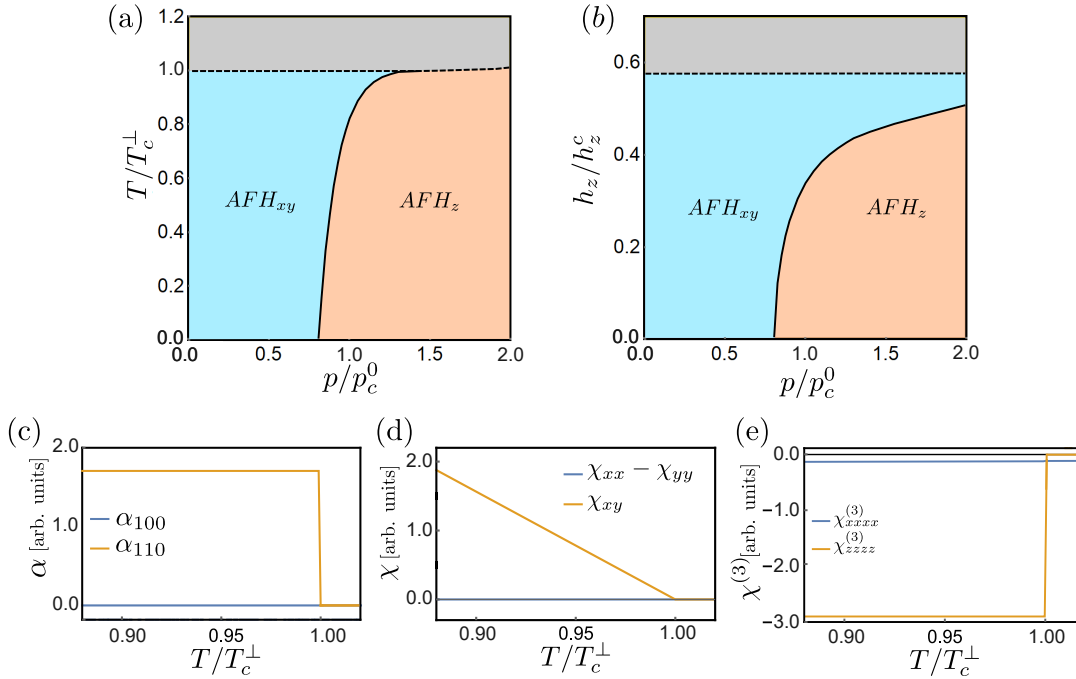
Figure 4: Antiferrohastatic phase diagrams in pressure and c-axis field, and thermodynamic responses across the AFH_{xy} transition. (a) Temperature versus pressure phase diagram in zero external field, where the dashed (solid) lines indicate second (first) order phase transitions. The AFH_{xy} phase captures the hidden order behavior, while the AFH_z phase behaves like the local moment antiferromagnet. (b) h_z field suppresses the c-axis AFH_z order in favour of AFH_{xy} order. (c) Thermal expansion jumps across $T_c^\perp$. (d) The basal plane susceptibility acquires a linear χ_{xy} below the transition. (e) The nonlinear susceptibility jumps show a large anisotropy, which is actually expected to be significantly larger for more realistic parameter choices.

The parameters given above reasonably reproduce the experimental phase diagrams in pressure and c-axis field, as shown in Fig. 4(a) and (b). We have also explored several characteristic response functions across the hastatic transitions, mainly anisotropic thermal expansion coefficients (α) and linear and nonlinear magnetic susceptibility matrix elements (χ and $\chi^{(3)}$), as well the magnetostriction tensor, but found that magnetostriction involved higher order effects that make it a much less sensitive probe. These response

functions are defined as follows (up to dimensionful constants for the thermal expansion):

$$\alpha_{100} = \frac{1}{L}\frac{\Delta L}{dT}\Big|_x - \frac{1}{L}\frac{\Delta L}{dT}\Big|_y \propto \frac{\partial R_{\Gamma_3}}{\partial T}, \tag{44}$$

$$\alpha_{110} = \frac{1}{L}\frac{\Delta L}{dT}\Big|_{[110]} - \frac{1}{L}\frac{\Delta L}{dT}\Big|_{[\bar{1}10]} \propto \frac{\partial R_{\Gamma_4}}{\partial T}, \tag{45}$$

$$\chi_{xx} - \chi_{yy} = -\frac{\partial^2 F}{\partial h_x^2} + \frac{\partial^2 F}{\partial h_y^2}, \quad \chi_{xy} = -\frac{\partial^2 F}{\partial h_x \partial h_y}, \tag{46}$$

$$\chi^{(3)}_{xxxx} = -\frac{\partial^4 F}{\partial h_x^4}, \quad \chi^{(3)}_{zzzz} = -\frac{\partial^4 F}{\partial h_z^4}. \tag{47}$$

The thermal expansion coefficients are a proxy for the elastic tetragonal symmetry breaking response and with the [110] pinning of the order parameter, there is a jump in α_{110}, as shown in Fig. 4 (c). As already noted in the main text, the jump is difficult to detect, due to $(T_{HO}/D)^2$ suppression of the elastic couplings ($\gamma_{3,4}$) and effects of multiple domains. The tetragonal symmetry breaking is also seen by the onset of χ_{xy} linear susceptibility, shown in Fig. 4 (d), however torque magnetometry measurements of χ_{xy} are more subtle and treated in the main text. Finally, the nonlinear susceptibility coefficients are shown in Fig. 4 (e), and exhibit a large Ising anisotropy due to the anisotropic field couplings, as has been observed experimentally [4].

The prediction of a thus far unobserved field-locking transition in large transverse fields provides a key experimental test for hastatic order. In the main text we treat the transition in a simplified model and here we show additional numerical results obtained by the optimization of the full free energy from Eq. (39)-(42) in Fig. 5.
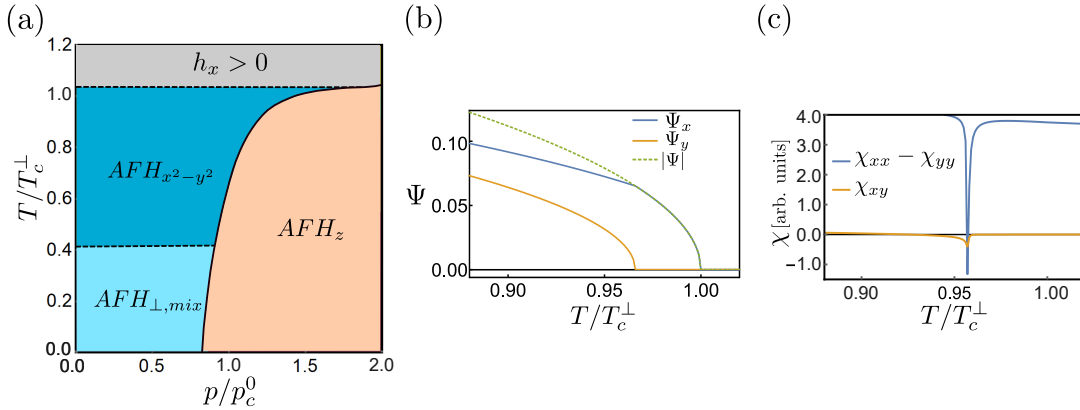
Figure 5: (a) p-T phase diagram in h_x field. The high temperature in-plane phase is field-locked ($AFH_{x^2-y^2}$), thus fully $\Psi^2_{\Gamma_3}$, while the low temperature phase ($AFH_{\perp,mix}$) is characterized by the onset of $\Psi^2_{\Gamma_4}$ component in a second order transition. (b) Order parameter components (Ψ_x and Ψ_y) show changes across both primary hastatic and field-locking transitions, while the overall magnitude changes changes significantly only for the main hastatic transition, with important consequences on bulk thermodynamic properties. (c) Susceptibility matrix elements showing divergence across field-locking transition. The change of slope of $\chi_{xx} - \chi_{yy}$ across the main transition is hard to distinguish due to the small size and originally non-zero $\chi_{xx} - \chi_{yy}$ in the presence of external h_x field. Parameters used for obtaining plots are standard quoted in this Appendix.

F Discussion of elastic coefficients and resonant ultrasound spectroscopy

Recent resonant ultrasound (RUS) experiments [18] set limits on the existence of two-component order parameters in URu_2Si_2 through the absence of observable jumps in symmetry breaking elastic coefficients. In this section, we argue that our two-component order parameter, $\vec{\Psi}_\perp$ lies comfortably within these limits and as such is not excluded as a hidden order candidate by RUS experiments.

As shown in [18], while any OP has jumps in the compressional (Γ_1) elastic moduli, only multi-component OPs lead to jumps in (Γ_3, Γ_4) shear moduli. The magnitudes of elastic moduli jumps (Δc_i) expected are proportional to the square of OP elastic couplings ($\gamma_{3,4}$ in our theory), more precisely from [18]:

$$\Delta c_{\Gamma_1} \sim \frac{\gamma_1^2}{u_\perp}, \qquad \Delta c_{\Gamma_3} \sim \frac{\gamma_3^2}{v_1}, \qquad \Delta c_{\Gamma_4} \sim \frac{\gamma_4^2}{u_\perp}. \qquad (48)$$

The denominator in the expressions above is closely related to the mass of the fluctuation field that couples linearly to the relevant strain component, thus Γ_3 strain has the weak transverse pinning, v_1 in the denominator.

From the microscopic theory, we expect that in the basal plane phases, $\gamma_{3,4}/\gamma_1 \sim (T_{HO}/D)^2$, and $v_1/u_\perp \sim (T_{HO}/D)^2$. While $\Delta c_{\Gamma_4}/\Delta c_{\Gamma_1} \sim (T_{HO}/D)^4$, due to small in-plane pinning, $\Delta c_{\Gamma_3}/\Delta c_{\Gamma_1} \sim (T_{HO}/D)^2$. $\Delta c_{\Gamma_3} = \Delta(c_{11} - c_{12})$ is therefore the largest predicted jump in our theory, but it is still suppressed by $(T_{HO}/D)^2 \sim .001$, corresponding to relative RUS frequency shifts of at best 10^{-8}, while detected Γ_1 jumps are $10^{-5} - 10^{-6}$ and the level of noise is at least 10^{-7}. Thus, even though the hastatic order parameter has multiple components, the weak coupling to the lattice ensures the absence of observable jumps in the shear elastic moduli.

G Nematic susceptibility

The nematic susceptibility associated with our two component in-plane order parameter has already been considered by [16], and so here we simply reproduce their calculations and discuss how it applies to our particular system. The nematic order parameter is the electronic manifestation of the broken tetragonal symmetry, and can generically be treated by adding the free energy,

$$F_\mathcal{N} = \frac{a_\mathcal{N}}{2}(T - T_\mathcal{N})\mathcal{N}^2 + \frac{b_\mathcal{N}}{4}\mathcal{N}^4 - \eta\mathcal{N}\epsilon_{\Gamma_4} - \zeta\mathcal{N}\Psi_{\Gamma_4}^2 \qquad (49)$$

Here, we have chosen the Γ_4 nematic order parameter associated with $\Psi_{\Gamma_4}^2$. It has an independent transition temperature, $T_\mathcal{N}$ that arises from fluctuations of $\vec{\Psi}_\perp$; in principle, $T_\mathcal{N}$ can be larger or smaller than T_{HO}, but here we assume that it is smaller. The relevant component of the elastoresistivity is proportional to the nematic susceptibility, $\partial\mathcal{N}/\partial\epsilon_{\Gamma_4}$, which contains a jump at T_{HO}. The nematic susceptibility is calculated by first solving $\partial F/\partial\Psi_{x,y} = 0$ for $\vec{\Psi}_\perp$ as a function of $\mathcal{N}$ and ϵ_{Γ_4}. This solution is inserted into the total free energy, and we then take $\partial F/\partial\mathcal{N} = 0$, and take $\partial/\partial\epsilon_{\Gamma_4}$ implicitly to solve for $\partial\mathcal{N}/\partial\epsilon_{\Gamma_4}$. As in [16], we find,

$$\chi_{nem} = \frac{\partial\mathcal{N}}{\partial\epsilon_{\Gamma_4}} = \begin{cases} \frac{\eta}{a_\mathcal{N}(T - T_\mathcal{N})} & T > T_{HO} \\ \frac{\eta + \frac{2\gamma_4\zeta}{4u_\perp - v_1}}{a_\mathcal{N}(T - T_\mathcal{N}) - \frac{2\zeta^2}{4u_\perp - v_1}} & T = T_{HO}^- \end{cases} . \qquad (50)$$

Below T_{HO}^-, the nematic order parameter, $\mathcal{N}$ also comes into the denominator and affects the temperature dependence, however, we are mainly interested in the jump. We can use the mean-field specific heat jump results, $\Delta C_V = \alpha_\perp^2/(8u_\perp - 2v_1)T_{HO}$ (or jump in $\partial \Psi_{\Gamma_4}^2/\partial T$ equivalently) to rewrite the jump in the nematic susceptibility to second order in γ_4 and ζ as,

$$\Delta \chi_{nem} = \frac{4\Delta C_V}{\alpha_\perp^2 T_{HO} a_{\mathcal{N}}(T - T_{\mathcal{N}})} \left[\gamma_4 \zeta + \frac{\eta \zeta^2}{a_{\mathcal{N}}(T - T_{\mathcal{N}})} \right] + \mathcal{O}\left(\gamma_4^2 \zeta^2, \zeta^3\right). \tag{51}$$

While the microscopics suggested that γ_4 is suppressed by $(T_{HO}/D)^2$, the electronic nematic order parameter associated with $\vec{\Psi}_\perp$ is expected to be of order one, as estimated by the tetragonal symmetry breaking distortion of the Fermi surface [33, 41]. Therefore the second term gives a significant jump in the elastoresistivity at T_{HO} that is significantly enhanced if $T_{\mathcal{N}}$ is close to T_{HO}. Note that this analysis is only for the main transition; the behavior will be different at the field-locking transition, for example, where the jump is no longer proportional to the (tiny) specific heat jump, but it is still related to the behaviour of $\partial \Psi_{\Gamma_i}^2/\partial T$.

References

[1] T. T. M. Palstra, A. A. Menovsky, J. van den Berg, A. J. Dirkmaat, P. H. Kes, G. J. Nieuwenhuys and J. A. Mydosh, *Superconducting and magnetic transitions in the heavy-fermion system URu_2Si_2*, Phys. Rev. Lett. **55**(24), 2727 (1985), doi:10.1103/PhysRevLett.55.2727.

[2] J. A. Mydosh and P. M. Oppeneer, *Colloquium: Hidden order, superconductivity, and magnetism: The unsolved case of URu_2Si_2*, Rev. Mod. Phys. **83**, 1301 (2011), doi:10.1103/RevModPhys.83.1301.

[3] M. M. Altarawneh, N. Harrison, S. E. Sebastian, L. Balicas, P. H. Tobash, J. D. Thompson, F. Ronning and E. D. Bauer, *Sequential spin polarization of the fermi surface pockets in URu_2Si_2 and its implications for the hidden order*, Phys. Rev. Lett. **106**(14), 146403 (2011), doi:10.1103/PhysRevLett.106.146403.

[4] J. Trinh, E. Brück, T. Siegrist, R. Flint, P. Chandra, P. Coleman and A. P. Ramirez, *Thermodynamic measurement of angular anisotropy at the hidden order transition of URu_2Si_2*, Phys. Rev. Lett. **117**, 157201 (2016), doi:10.1103/PhysRevLett.117.157201.

[5] A. R. Schmidt, M. H. Hamidian, P. Wahl, F. Meier, A. V. Balatsky, J. D. Garrett, T. J. Williams, G. M. Luke and J. C. Davis, *Imaging the fano lattice to hidden order transition in URu_2Si_2*, Nature **465**(7298), 570 (2010), doi:10.1038/nature09073.

[6] P. Aynajian, E. H. Da Silva Neto, C. V. Parker, Y. Huang, A. Pasupathy, J. Mydosh and A. Yazdania, *Visualizing the formation of the Kondo lattice and the hidden order in URu_2Si_2*, Proc. Natl. Acad. Sci. U. S. A. **107**(23), 10383 (2010), doi:10.1073/pnas.1005892107.

[7] U. Nagel, T. Uleksin, T. Rõõm, R. P. Lobo, P. Lejay, C. C. Homes, J. S. Hall, A. W. Kinross, S. K. Purdy, T. Munsie, T. J. Williams, G. M. Luke *et al.*, *Optical spectroscopy shows that the normal state of URu_2Si_2 is an anomalous Fermi liquid*, Proc. Natl. Acad. Sci. U. S. A. **109**(47), 19161 (2012), doi:10.1073/pnas.1208249109.

[8] S. Zhang, G. Chappell, N. Pouse, R. E. Baumbach, M. B. Maple, L. H. Greene and W. K. Park, *Origin of gaplike behaviors in URu_2Si_2: Combined study via quasiparticle scattering spectroscopy and resistivity measurements*, Phys. Rev. B **102**, 081101(R) (2020), doi:10.1103/PhysRevB.102.081101.

[9] J.-Q. Meng, P. M. Oppeneer, J. A. Mydosh, P. S. Riseborough, K. Gofryk, J. J. Joyce, E. D. Bauer, Y. Li and T. Durakiewicz, *Imaging the three-dimensional fermi-surface pairing near the hidden-order transition in URu_2Si_2 using angle-resolved photoemission spectroscopy*, Phys. Rev. Lett. **111**, 127002 (2013), doi:10.1103/PhysRevLett.111.127002.

[10] A. Villaume, F. Bourdarot, E. Hassinger, S. Raymond, V. Taufour, D. Aoki and J. Flouquet, *Signature of hidden order in heavy fermion superconductor URu_2Si_2: Resonance at the wave vector $Q_0 = (1,0,0)$*, Phys. Rev. B **78**, 012504 (2008), doi:10.1103/PhysRevB.78.012504.

[11] E. Hassinger, G. Knebel, T. D. Matsuda, D. Aoki, V. Taufour and J. Flouquet, *Similarity of the fermi surface in the hidden order state and in the antiferromagnetic state of URu_2Si_2*, Phys. Rev. Lett. **105**, 216409 (2010), doi:10.1103/PhysRevLett.105.216409.

[12] E. R. Schemm, R. E. Baumbach, P. H. Tobash, F. Ronning, E. D. Bauer and A. Kapitulnik, *Evidence for broken time-reversal symmetry in the superconducting phase of URu_2Si_2*, Phys. Rev. B **91**(14), 140506(R) (2015), doi:10.1103/PhysRevB.91.140506.

[13] H.-H. Kung, R. E. Baumbach, E. D. Bauer, V. K. Thorsmølle, W.-L. Zhang, K. Haule, J. A. Mydosh and G. Blumberg, *Chirality density wave of the "hidden order" phase in URu_2Si_2*, Science **347**(6228), 1339 (2015), doi:10.1126/science.1259729.

[14] R. Okazaki, T. Shibauchi, H. J. Shi, Y. Haga, T. D. Matsuda, E. Yamamoto, Y. Onuki, H. Ikeda and Y. Matsuda, *Rotational symmetry breaking in the hidden-order phase of URu_2Si_2*, Science **331**(6016), 439 (2011), doi:10.1126/science.1197358.

[15] S. Tonegawa, S. Kasahara, T. Fukuda, K. Sugimoto, N. Yasuda, Y. Tsuruhara, D. Watanabe, Y. Mizukami, Y. Haga, T. D. Matsuda, E. Yamamoto, Y. Onuki *et al.*, *Direct observation of lattice symmetry breaking at the hidden-order transition in URu_2Si_2*, Nat. Commun. **5**(1), 4188 (2014), doi:10.1038/ncomms5188.

[16] S. C. Riggs, M. C. Shapiro, A. V. Maharaj, S. Raghu, E. D. Bauer, R. E. Baumbach, P. Giraldo-Gallo, M. Wartenbe and I. R. Fisher, *Evidence for a nematic component to the hidden-order parameter in URu_2Si_2 from differential elastoresistance measurements*, Nat. Commun. **6**(1), 6425 (2015), doi:10.1038/ncomms7425.

[17] J. Choi, O. Ivashko, N. Dennler, D. Aoki, K. Von Arx, S. Gerber, O. Gutowski, M. H. Fischer, J. Strempfer, M. V. Zimmermann and J. Chang, *Pressure-induced rotational symmetry breaking in URu_2Si_2*, Phys. Rev. B **98**(24), 241113(R) (2018), doi:10.1103/PhysRevB.98.241113.

[18] S. Ghosh, M. Matty, R. Baumbach, E. D. Bauer, K. A. Modic, A. Shekhter, J. A. Mydosh, E.-A. Kim and B. J. Ramshaw, *One-component order parameter in URu_2Si_2 uncovered by resonant ultrasound spectroscopy and machine learning*, Sci. Adv. **6**(10) (2020), doi:10.1126/sciadv.aaz4074.

[19] L. Wang, M. He, F. Hardy, D. Aoki, K. Willa, J. Flouquet and C. Meingast, *Electronic nematicity in URu_2Si_2 revisited*, Phys. Rev. Lett. **124**, 257601 (2020), doi:10.1103/PhysRevLett.124.257601.

[20] H. Amitsuka and T. Sakakibara, *Single uranium-site properties of the dilute heavy electron system $U_x Th_{1-x} Ru_2 Si_2$ ($x \leq 0.07$)*, J. Phys. Soc. Jpn. **63**(2), 736 (1994), doi:10.1143/JPSJ.63.736.

[21] K. Haule and G. Kotliar, *Arrested kondo effect and hidden order in $URu_2 Si_2$*, Nat. Phys. **5**(11), 796 (2009), doi:10.1038/nphys1392.

[22] P. Santini and G. Amoretti, *Crystal field model of the magnetic properties of $URu_2 Si_2$*, Phys. Rev. Lett. **73**, 1027 (1994), doi:10.1103/PhysRevLett.73.1027.

[23] C. M. Varma and L. Zhu, *Helicity order: Hidden order parameter in $URu_2 Si_2$*, Phys. Rev. Lett. **96**, 036405 (2006), doi:10.1103/PhysRevLett.96.036405.

[24] C. Pépin, M. R. Norman, S. Burdin and A. Ferraz, *Modulated spin liquid: A new paradigm for $URu_2 Si_2$*, Phys. Rev. Lett. **106**, 106601 (2011), doi:10.1103/PhysRevLett.106.106601.

[25] Y. Dubi and A. V. Balatsky, *Hybridization wave as the "hidden order" in $URu_2 Si_2$*, Phys. Rev. Lett. **106**, 086401 (2011), doi:10.1103/PhysRevLett.106.086401.

[26] S. Fujimoto, *Spin nematic state as a candidate of the hidden order phase of $URu_2 Si_2$*, Phys. Rev. Lett. **106**, 196407 (2011), doi:10.1103/PhysRevLett.106.196407.

[27] H. Ikeda, M.-T. Suzuki, R. Arita, T. Takimoto, T. Shibauchi and Y. Matsuda, *Emergent rank-5 nematic order in $URu_2 Si_2$*, Nat. Phys. **8**(7), 528 (2012), doi:10.1038/nphys2330.

[28] P. M. Oppeneer, S. Elgazzar, J. Rusz, Q. Feng, T. Durakiewicz and J. A. Mydosh, *Spin and orbital hybridization at specifically nested fermi surfaces in $URu_2 Si_2$*, Phys. Rev. B **84**, 241102(R) (2011), doi:10.1103/PhysRevB.84.241102.

[29] T. Yuan, J. Figgins and D. K. Morr, *Hidden order transition in $URu_2 Si_2$: Evidence for the emergence of a coherent anderson lattice from scanning tunneling spectroscopy*, Phys. Rev. B **86**, 035129 (2012), doi:10.1103/PhysRevB.86.035129.

[30] J. G. Rau and H.-Y. Kee, *Hidden and antiferromagnetic order as a rank-5 superspin in $URu_2 Si_2$*, Phys. Rev. B **85**, 245112 (2012), doi:10.1103/PhysRevB.85.245112.

[31] P. Chandra, P. Coleman and R. Flint, *Hastatic order in the heavy-fermion compound $URu_2 Si_2$*, Nature **493**(7434), 621 (2013), doi:10.1038/nature11820.

[32] C.-H. Hsu and S. Chakravarty, *Superconductivity from fractionalized excitations in $URu_2 Si_2$*, Phys. Rev. B **90**, 134507 (2014), doi:10.1103/PhysRevB.90.134507.

[33] P. Chandra, P. Coleman and R. Flint, *Hastatic order in $URu_2 Si_2$: Hybridization with a twist*, Phys. Rev. B **91**(20), 205103 (2015), doi:10.1103/PhysRevB.91.205103.

[34] W. K. Park, P. H. Tobash, F. Ronning, E. D. Bauer, J. L. Sarrao, J. D. Thompson and L. H. Greene, *Observation of the hybridization gap and fano resonance in the Kondo lattice $URu_2 Si_2$*, Phys. Rev. Lett. **108**(24), 246403 (2012), doi:10.1103/PhysRevLett.108.246403.

[35] H. Ohkuni, Y. Inada, Y. Tokiwa, K. Sakurai, R. Settai, T. Honma, Y. Haga, E. Yamamoto, Y. Ōnuki, H. Yamagami, S. Takahashi and T. Yanagisawa, *Fermi surface properties and de Haas–van Alphen oscillation in both the normal and superconducting mixed states of $URu_2 Si_2$*, Philos. Mag. B **79**(7), 1045 (1999), doi:10.1080/13642819908214859.

[36] G. Bastien, D. Aoki, G. Lapertot, J. P. Brison, J. Flouquet and G. Knebel, *Fermi-surface selective determination of the g-factor anisotropy in URu_2Si_2*, Phys. Rev. B **99**(16), 165138 (2019), doi:10.1103/PhysRevB.99.165138.

[37] N. Metoki, H. Sakai, E. Yamamoto, N. Tateiwa, T. Matsuda and Y. Haga, *Neutron scattering experiments for the study of in-plane ordered moment in URu_2Si_2*, J. Phys. Soc. Japan **82**(5), 055004 (2013), doi:10.7566/JPSJ.82.055004.

[38] P. Das, R. E. Baumbach, K. Huang, M. B. Maple, Y. Zhao, J. S. Helton, J. W. Lynn, E. D. Bauer and M. Janoschek, *Absence of a static in-plane magnetic moment in the 'hidden-order' phase of URu_2Si_2*, New J. Phys. **15**, 053031 (2013), doi:10.1088/1367-2630/15/5/053031.

[39] K. A. Ross, L. Harriger, Z. Yamani, W. J. L. Buyers, J. D. Garrett, A. A. Menovsky, J. A. Mydosh and C. L. Broholm, *Strict limit on in-plane ordered magnetic dipole moment in URu_2Si_2*, Phys. Rev. B **89**(15), 155122 (2014), doi:10.1103/PhysRevB.89.155122.

[40] F. Bridges, R. Dudschus, C. Mackeen, T. Keiber, C. H. Booth and M. B. Maple, *EXAFS investigation of the local structure in $URu_{2-x}Fe_xSi_2$: Evidence for distortions below 100 K*, Phys. Rev. B **102**, 014109 (2020), doi:10.1103/PhysRevB.102.014109.

[41] *No Title*, M. Kornjaca and R. Flint, in preparation.

[42] O. O. Bernal, M. E. Moroz, H. G. Lukefahr, D. E. MacLaughlin, J. A. Mydosh, A. A. Menovsky and C. Ortiz, *Ambient-pressure ^{99}Ru NMR in URu_2Si_2: Internal-field anisotropy*, J. Magn. Magn. Mater. **272-276**(SUPPL. 1), E59 (2004), doi:10.1016/j.jmmm.2003.11.159.

[43] S. Takagi, S. Ishihara, M. Yokoyama and H. Amitsuka, *Symmetry of the hidden order in URu_2Si_2 from nuclear magnetic resonance studies*, J. Phys. Soc. Japan **81**(11), 114710 (2012), doi:10.1143/JPSJ.81.114710.

[44] P. Coleman and N. Andrei, *Kondo-stabilised spin liquids and heavy fermion superconductivity*, J. Phys. Condens. Matter **1**(26), 4057 (1989), doi:10.1088/0953-8984/1/26/003.

[45] T. Senthil, S. Sachdev and M. Vojta, *Fractionalized fermi liquids*, Phys. Rev. Lett. **90**, 216403 (2003), doi:10.1103/PhysRevLett.90.216403.

[46] S. Hoshino, J. Otsuki and Y. Kuramoto, *Diagonal composite order in a two-channel kondo lattice*, Phys. Rev. Lett. **107**, 247202 (2011), doi:10.1103/PhysRevLett.107.247202.

[47] S. Hoshino, J. Otsuki and Y. Kuramoto, *Resolution of entropy $\ln\sqrt{2}$ by ordering in two-channel kondo lattice*, J. Phys. Soc. Jpn. **82**(4), 044707 (2013), doi:10.7566/JPSJ.82.044707.

[48] Y. Komijani, A. Toth, P. Chandra and P. Coleman, *Order fractionalization*, arXiv (2019).

[49] A. Wugalter, Y. Komijani and P. Coleman, *Large-N approach to the two-channel Kondo lattice*, Phys. Rev. B **101**, 075133 (2020), doi:10.1103/PhysRevB.101.075133.

[50] G. Zhang, J. S. Van Dyke and R. Flint, *Cubic hastatic order in the two-channel Kondo-Heisenberg model*, Phys. Rev. B **98**(23), 235143 (2018), doi:10.1103/PhysRevB.98.235143.

[51] H. Amitsuka, M. Sato, N. Metoki, M. Yokoyama, K. Kuwahara, T. Sakakibara, H. Morimoto, S. Kawarazaki, Y. Miyako and J. A. Mydosh, *Effect of pressure on tiny anti-ferromagnetic moment in the heavy-electron compound URu_2Si_2*, Phys. Rev. Lett. **83**, 5114 (1999), doi:10.1103/PhysRevLett.83.5114.

[52] P. G. Niklowitz, C. Pfleiderer, T. Keller, M. Vojta, Y.-K. Huang and J. A. Mydosh, *Parasitic small-moment antiferromagnetism and nonlinear coupling of hidden order and antiferromagnetism in URu_2Si_2 observed by larmor diffraction*, Phys. Rev. Lett. **104**, 106406 (2010), doi:10.1103/PhysRevLett.104.106406.

[53] S. Tonegawa, K. Hashimoto, K. Ikada, Y. H. Lin, H. Shishido, Y. Haga, T. D. Matsuda, E. Yamamoto, Y. Onuki, H. Ikeda, Y. Matsuda and T. Shibauchi, *Cyclotron resonance in the hidden-order phase ofURu_2Si_2*, Phys. Rev. Lett. **109**(3), 036401 (2012), doi:10.1103/PhysRevLett.109.036401.

[54] Y. J. Jo, L. Balicas, C. Capan, K. Behnia, P. Lejay, J. Flouquet, J. A. Mydosh and P. Schlottmann, *Field-induced fermi surface reconstruction and adiabatic continuity between antiferromagnetism and the hidden-order state in URu_2Si_2*, Phys. Rev. Lett. **98**, 166404 (2007), doi:10.1103/PhysRevLett.98.166404.

[55] M. A. López de la Torre, S. Vieira, R. Villar, M. B. Maple and M. S. Torikachvili, *Low temperature specific heat of URu_2Si_2 near the superconducting transition*, Phys. B Phys. Condens. Matter **165-166**(PART 1), 385 (1990), doi:10.1016/S0921-4526(90)81042-M.

[56] A. Gallagher, K. W. Chen, C. M. Moir, S. K. Cary, F. Kametani, N. Kikugawa, D. Graf, T. E. Albrecht-Schmitt, S. C. Riggs, A. Shekhter and R. E. Baumbach, *Unfolding the physics of URu_2Si_2 through silicon to phosphorus substitution*, Nat. Commun. **7**, 10712 (2016), doi:10.1038/ncomms10712.

[57] J. Lou, A. W. Sandvik and L. Balents, *Emergence of U(1) symmetry in the 3D XY model with Z_q anisotropy*, Phys. Rev. Lett. **99**, 207203 (2007), doi:10.1103/PhysRevLett.99.207203.

[58] Y. Imry and S.-k. Ma, *Random-field instability of the ordered state of continuous symmetry*, Phys. Rev. Lett. **35**, 1399 (1975), doi:10.1103/PhysRevLett.35.1399.

[59] M. Aizenman and J. Wehr, *Rounding of first-order phase transitions in systems with quenched disorder*, Phys. Rev. Lett. **62**, 2503 (1989), doi:10.1103/PhysRevLett.62.2503.

[60] T. Nattermann, *Theory of Random Field Ising Model*, pp. 277–298, World Scientific, doi:10.1142/9789812819437_0009 (1997).

[61] R. Fisch, *Random-field models for relaxor ferroelectric behavior*, Phys. Rev. B **67**, 094110 (2003), doi:10.1103/PhysRevB.67.094110.

[62] L. Nie, G. Tarjus and S. A. Kivelson, *Quenched disorder and vestigial nematicity in the pseudogap regime of the cuprates*, Proc. Natl. Acad. Sci. U. S. A. **111**(22), 7980 (2014), doi:10.1073/pnas.1406019111.

[63] I. Kawasaki, I. Watanabe, A. Hillier and D. Aoki, *Time-reversal symmetry in the hidden order and superconducting states of URu_2Si_2*, J. Phys. Soc. Jpn. **83**(9), 094720 (2014), doi:10.7566/JPSJ.83.094720.

[64] K. Matsubayashi, T. Tanaka, A. Sakai, S. Nakatsuji, Y. Kubo and Y. Uwatoko, *Pressure-induced heavy fermion superconductivity in the nonmagnetic quadrupolar system $PrTi_2Al_2$*, Phys. Rev. Lett. **109**(18), 187004 (2012), doi:10.1103/PhysRevLett.109.187004.

[65] J. S. Van Dyke, G. Zhang and R. Flint, *Field-induced ferrohastatic phase in cubic non-Kramers doublet systems*, Phys. Rev. B **100**(20), 205122 (2019), doi:10.1103/PhysRevB.100.205122.

[66] S. Ran, I. Jeon, N. Pouse, A. J. Breindel, N. Kanchanavatee, K. Huang, A. Gallagher, K. W. Chen, D. Graf, R. E. Baumbach, J. Singleton and M. B. Maple, *Phase diagram of $URu_{2-x}Fe_xSi_2$ in high magnetic fields*, Proc. Natl. Acad. Sci. U. S. A. **114**(37), 9826 (2017), doi:10.1073/pnas.1710192114.

[67] W. Knafo, S. Araki, G. Lapertot, D. Aoki, G. Knebel and D. Braithwaite, *Destabilization of hidden order in URu_2Si_2 under magnetic field and pressure*, Nat. Phys. **16**(9), 942 (2020), doi:10.1038/s41567-020-0927-4.